MAGNETIC INVESTIGATIONS
ON SOME RARE-EARTH CHALCOGENIDES

J. W. ARBOUW

MAGNETIC INVESTIGATIONS

ON SOME RARE-EARTH

CHALCOGENIDES

PROEFSCHRIFT

TER VERKRIJGING VAN DE GRAAD VAN DOCTOR IN
DE WISKUNDE EN NATUURWETENSCHAPPEN AAN DE
RIJKSUNIVERSITEIT TE LEIDEN, OP GEZAG VAN DE
RECTOR MAGNIFICUS DR. A.E. COHEN, HOOGLERAAR
IN DE FACULTEIT DER LETTEREN, VOLGENS
BESLUIT VAN HET COLLEGE VAN DEKANEN TE
VERDEDIGEN OP WOENSDAG 2 OKTOBER 1974
TE KLOKKE 15.15 UUR

door

JAN WOUTER ARBOUW
geboren te LEIDEN in 1941

STELLINGEN

1. De conclusie van Kobayashi, Tsujikawa en Friedberg dat een spingolf model toegepast op een ééndimensionaal magnetisch systeem de waarde van $\chi_\perp(0)$ voor de magnetische keten verbinding $CsMnCl_3 \cdot 2H_2O$ bevredigend verklaart is niet afdoende gefundeerd.

    H. Kobayashi, I. Tsujikawa en S.A. Friedberg, J. Low Temp. Phys. <u>10</u>, 621 (1973).

2. Door aan te nemen dat bij 250 $^\circ$C de methaan-deuterium uitwisseling op 2% Ni/SiO_2 uitsluitend op het nikkel plaats heeft, gaan Cece en Gonzales ten onrechte voorbij aan eerder door henzelf verkregen resultaten.

    J.M. Cece en R.D. Gonzales, J. Catal. <u>28</u>, 260 (1973).

    J.M. Cece en R.D. Gonzales, J. Catal. <u>28</u>, 254 (1973).

3. De interpretatie van de absorptiebanden in het spectrum van mangaan-cupferraat zoals die gegeven wordt door Abou El Ela en Afifi stemt niet overeen met de toekenning van de absorptiebanden van het door dezelfde auteurs beschreven zinkcupferraat-complex.

    A.H. Abou El Ela en H.H. Afifi, Z. naturforsch. <u>29a</u>, 719 (1974).

4. De toekenning in de NMR spectra van p-halogeenfenyllood-tris (trifluor-acetaat) aan de fenylprotonen zijn door Kalman, Pinhey en Sternhell onzorgvuldig gedaan.

    J.R. Kalman, J.T. Pinhey en S. Sternhell, Tetrahedron Letters <u>5</u>, 5369 (1972).

5. De conclusie van Clack en Williams dat de resultaten van nun M.O. berekeningen aan CuF_6^{2-} worden ondersteund door de door hen gemeten absorptiespectra is aan twijfel onderhevig.

    D.W. Clack en W.T. Williams, J. Inorg. Nucl. Chem. <u>35</u>, 3535 (1973).

6. De indicering van het röntgendiffractiepatroon van $NaMnCl_3$ zoals die door Kestigian en Croft voor het door hen bereide preparaat gegeven wordt is onjuist.

    M. Kestigian en W.J. Croft, Mat. Res. Bull. <u>4</u>, 877 (1969)

7. De conclusie van Riou, Gérault en Lecerf dat de zuurstofatomen en de OH-groepen in het γ-$Cu_2(OH)_2CrO_4$ een hexagonale dichtste bolstapel vormen is onjuist.

   A. Riou, Y. Gérault en A. Lecerf, Bull. Soc. France Min. Crist. 96, 25 (1973).

8. De door Yu.E. Kirsh, O.P. Komarova en G.M. Lukovkin gevestigde indruk dat het potentiometrisch titratiegedrag van poly-4-vinyl-pyridine als functie van de zoutconcentratie in het gebied van lage ladingsdichtheid afwijkt van het gedrag van andere zwakke polyelectrolyten is onjuist.

   Yu.E. Kirsh, O.P. Komarova en G.M. Lukovkin, European Polymer J. 9, 1405 (1973).

9. Aangezien een mede-eigenaar van een octrooi volgens artikel 39 lid 2 van de Rijksoctrooiwet de bevoegdheid heeft alle handelingen genoemd in artikel 30 van de Rijksoctrooiwet te verrichten, kan, omdat uit artikel 39 lid 1 van de Rijksoctrooiwet en uit de Memorie van Toelichting daarop blijkt dat de mede-eigendom van een octrooi een vrije mede-eigendom is, het gedeelte van artikel 39 lid 2 van de Rijksoctrooiwet, waarin bepaald wordt dat licentie slechts met gemeen goedvinden der mede-eigenaren verleend kan worden, tot een dode letter gemaakt worden door overdracht van een gedeelte van een aandeel in een octrooi.

10. Het zou aanbeveling verdienen voor die ongehuwde en andere alleenstaanden die daar prijs op stellen de mogelijkheid te scheppen met vervroegd pensioen te gaan.

11. Gezien het feit dat de gemiddelde levensduur van vrouwen groter is dan die van mannen, is het onrechtvaardig vrouwen op een lagere leeftijd te pensioneren.

J.W. Arbouw   Leiden, 2 oktober 1974

CONTENTS

Aan mijn ouders

Voor Henny

CONTENTS

CONTENTS

CHAPTER I

INTRODUCTION

During the past decade a lot of information has been obtained in the field of the chemistry and physics of the rare-earth metals. One of the reasons for this is the availability of the rare-earth metals and a great number of their compounds in a high state of purity and at reasonable prices.

From a crystal chemical point of view the rare-earth metals and compounds are very interesting because in corresponding valence states the ionic radius decreases with increasing atomic number. This gives the crystal chemist the possibility to search after the influence of the radius ratio of cation and anion on the crystal structure, and related to that after the influence of the radius ratio on the physical properties.

From a physical point of view the rare-earth metals and compounds are also of great interest because of the, by the outer 5s- and 5p-electrons well screened, 4f-electrons which are responsible for the greater part of the magnetical and other physical properties.

The ground states of the trivalent rare-earth ions are in general very well described by the Russell-Saunders coupling model, and the values of the effective magnetic moments (μ_{eff}) are generally in good agreement with the theoretical values $\mu_{eff} = g\sqrt{J(J + 1)} \ \mu_B$, where g is the Landé spectroscopic splitting factor and J is the total angular momentum. Only in the cases of Eu(III) and Sm(III) there is a discrepancy which can be explained by the existence of excited states lying close enough to the ground state to be populated at ordinary temperatures.

The behaviour of the rare-earth ions is obviously different from

7

the magnetic behaviour of the compounds of the first row transition metals. In compounds of these elements the influence of the crystal field on the atomic orbitals of the magnetic ions is much greater and consequently the orbital angular momentum is completely or partially quenched. In many of these compounds the effective magnetic moment is fairly well described by: $\mu_{eff} = g\sqrt{S(S + 1)}\ \mu_B$, where S is the spin angular momentum, and g is not greatly different from the "free-electron" value of 2 (deviations up to 20% due to residual orbital contributions may occur).

Next to the difference in magnetic behaviour of the rare-earth compounds from that of the first row transition metal compounds, the magnetic behaviour of the rare-earth metals and alloys also differs from that of the other spontaneously magnetized elements, iron, cobalt and nickel.

The magnetic moment of the spontaneously magnetized rare-earth metals results mainly from the 4f-electrons, which are localized at the individual ions. This is clearly revealed: first by the measurements of the magnetic moment per ion determined by saturation measurements second by measurements of the paramagnetic susceptibility well above the magnetic ordering temperatures. These moments correspond, in most cases, within a few percent with the theoretical values for isolated rare-earth ions having unpaired 4f-electrons, as is indicated in table I-1.

As in the case of iron, cobalt and nickel the direct 3d-3d exchange interaction is too weak to account for the magnetic ordering (1), the even much weaker 4f-4f exchange interaction is incapable to explain the magnetic ordering in rare-earth metals at a somewhat elevated temperature. Therefore it is reasonable that other electrons than the localized 4f-electrons are assumed to take part in the interaction even though they make only a small contribution to the spontaneous magnetic moment. That a different type of magnetic interaction plays a role here is also indicated in table I-1, where the different kinds of spin-arrangements are also listed.

Zener (2) proposed a model of magnetic interaction in which itinerant electrons couple together electrons which are localized on

Metal	T_λ (K)	T_N (K)	T_C (K)	Θ_p (K)	$\mu_m(\mu_B)$	$\mu_{eff}(\mu_B)$	Spin Arrangement
Ce	12.5	12.5			0.62(2.14)		
Nd	19	20			2.3 (3.27)		
	7.2		7.5		1.8		
Sm	13.6	14.8					
Eu		90			5.9 (7.0)		
Gd	291		293.2	$\Theta_{//} = \Theta_\perp = 317$	7.55(7.0)	7.97(7.94)	Ferro.
Tb	227.7	229		$\Theta_{//} = 195 \quad \Theta_\perp = 239$	9.34(9.0)	9.70(9.72)	Spiral.
	221		221				Ferro.
Dy	174	178.5		$\Theta_{//} = 121 \quad \Theta_\perp = 169$	10.20(10.0)	10.64(10.65)	Spiral.
	83.5		85				Ferro.
Ho	131.6	132		$\Theta_{//} = 73 \quad \Theta_\perp = 88$	10.34(10.0)		Spiral.
	19.4		20				Ferro.
Er	84	85		$\Theta_{//} = 61.7 \quad \Theta_\perp = 32.5$	8.0 (9.0)		Sinusoidal.
	53.5						Spiral.
	19.9		19.6				Ferro.
Tm	55	53		$\Theta = 20$	6.8 (7.0)		Ferro.
			22				4,3,4,3-Ferro.

Table I-1. Some magnetical properties of the rare-earth metals. T_λ anomalies in the specific heat, T_N: Néel temperature, T_C: Curie temperature, Θ_p: paramagnetic Curie temperature, μ_m: saturation moment, μ_{eff}: effective magnetic moment, the values in parenthesis are the calculated values. (After W.C. Koehler (18).)

the rare-earth ions. Ruderman and Kittel (3) worked out a similar
second order interaction between nuclear spins via the conduction elec-
trons. Kasuya (4) and Yosida (5) obtained for the coupling of localized
ionic moments via the conduction electrons a similar quantitative result.
This theory, the so-called Ruderman and Kittel, Kasuya and Yosida
(RKKY) theory can be used to explain many of the properties of the rare-
earth metals and their alloys (6-13).

The magnetic behaviour of the insulating rare-earth compounds
generally can be explained in terms of a weak direct and a weak
super exchange interaction. E.g. the magnetic properties in the series
EuO, EuS, EuSe and EuTe; in which the oxide, sulphide and selenide of
europium are ferromagnetic, and EuTe is antiferromagnetic (Gorter et
al. (14))(table I-2). The direct exchange interaction in these compounds

	μ_{eff}	μ_m	Θ_p (K)	T_C (K)
EuO	7.9	6.9		+77
EuS	8.0	6.5	+16	+16
EuSe	8.2	7.0	+ 6	+ 6
EuTe	7.6		- 7.5	+11

Table I-2. Magnetic data for europium
chalcogenides. (After E.W.
Gorter et al. (14).)

is assumed to be ferromagnetic and to decrease with increasing cell-
edge; the super exchange interaction via an anion is supposed to be
antiferromagnetic and to increase with increasing atomic number of the
anion.

F. Holtzberg et al. (15) suggested that the magnetic properties
of the series $Eu_{(1-x)}Gd_xSe$ (x = 0 to 1), which form a complete homo-
geneous system having the rocksalt structure and a number of conduction
electrons per magnetic ion that varies from 1 for x = 1 to 0 for x = 0,
can be explained in terms of the RKKY-theory. This applies as well for

the series $Eu_{(1-x)}La_xSe$ with the same variation in conduction electron concentration and with a varying number of magnetic ions. As in the weak ferromagnetic semiconductor EuSe the Eu(II) ions are partially replaced by Gd(III) or La(III) ions the number of electrons in the conduction band increases. In addition to a large increase in electrical conductivity the paramagnetic Curie-temperature (θ_p) changes from positive to negative in the case of the system $Eu_{(1-x)}Gd_xSe$. In the system $Eu_{(1-x)}La_xSe$, the paramagnetic Curie-temperature has the same behaviour, but the changes are less due to the decrease in number of the magnetic ions. Figure I-1 gives the paramagnetic Curie-temperature
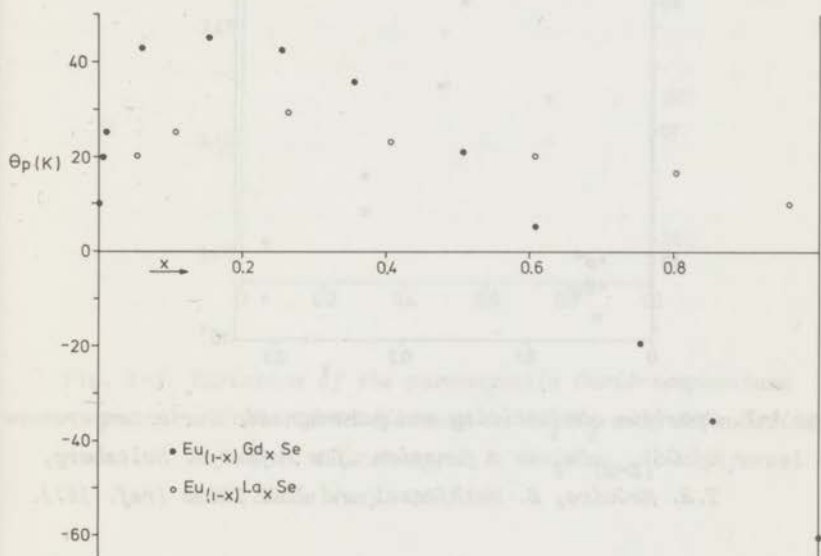
Fig. I-1. *Variation of the paramagnetic Curie-temperature of EuSe with Gd(III) and La(III) substitution (after F. Holtzberg, T.R. McGuire, S. Methfessel and J.C. Suits (ref. 15)).*

versus x for these two series.

The same authors (16) indicated that probably a similar interaction occurred in the gadolinium selenide series $Gd_{(3-x)}Se_4$, where $x = 0$ to 1/3, with the thorium phosphide structure (figure I-2), and

11
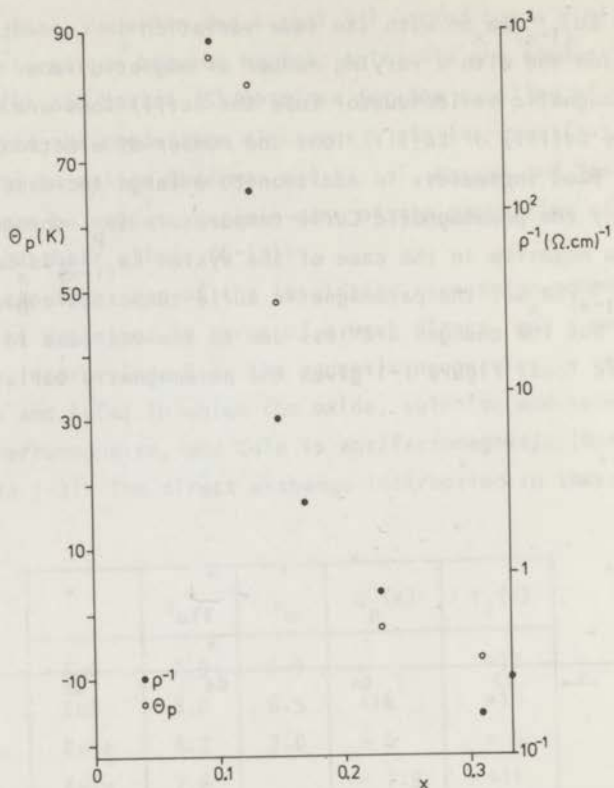
Fig. I-2. *Specific conductivity and paramagnetic Curie-temperature of $Gd_{(3-x)}Se_4$ as a function of x (after F. Holtzberg, T.R. McGuire, S. Methfessel and J.C. Suits (ref. 16)).*

in the mixed gadolinium antimonide-gadolinium bismuthide system of the formula $Gd_4(Sb_xBi_{(1-x)})_3$, (x = 0 to 1), with the anti-thorium phosphide structure (figure I-3).

J. Grunzweig and M. Kuznietz (17) tried to account for the proper-ties of uranium compounds UX, where X is either an element of the pnictide group (N,P,As,Sb) or an element of the chalcogenide group (S,Se,Te). The pnictide group compounds are antiferromagnetic, while the chalcogenide group compounds are ferromagnetic. All compounds have the rocksalt structure, high magnetic transition temperatures (50 - 220 K) and low electrical resistivities (table I-3). The uranium ion
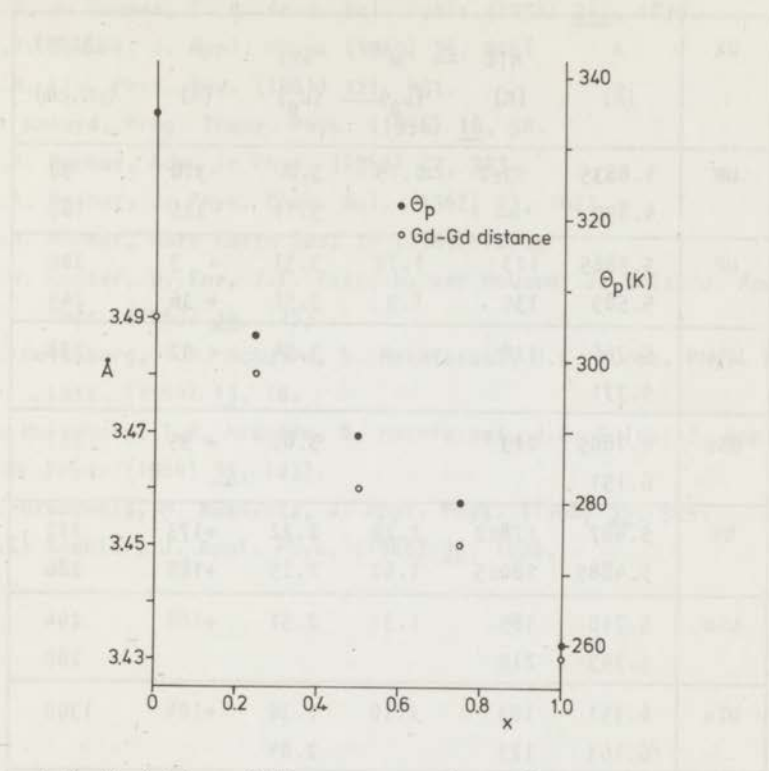
Fig. 1-3. *Variation of the paramagnetic Curie-temperature and the Gd-Gd distance in Gd_4Bi_3 with Sb substitution (after F. Holtzberg, T.R. McGuire, S. Methfessel and J.C. Suits (ref. 16)).*

is assumed to be in the U(IV) state and the surplus electrons are supposed to be in a conduction band. The coupling between U(IV) ions is assumed to be an indirect one via the conduction electrons (RKKY mechanism). The experimental data agree rather well with these assumptions.

13

UX	a (Å)	$T_{N,C}$ (K)	μ_m (μ_B)	μ_{eff} (μ_B)	Θ (K)	ρ (300K) ($\mu\Omega\cdot$cm)
UN	4.8835	53±2	0.75	3.0	-310	90
	4.890			3.11	-325	160
UP	5.5865	123	1.72	3.31	+ 3	200
	5.589	130	1.9	3.56	+ 36	244
UAs	5.766	128		3.54	+ 32	238
	5.771					
USb	6.1805	213		3.85	+ 95	357
	6.191					
US	5.487	178±2	1.20	2.22	+173	112
	5.4885	180±5	1.60	2.25	+185	286
USe	5.710	185	1.31	2.51	+188	244
	5.743	210				280
UTe	6.151	103	1.10	2.36	+104	1300
	6.163	123		2.84		

Table I-3. Properties of UX compounds (after J. Grunzweig and M. Kuznietz (17)).

References

1. R.N. Stuart, W. Marshall, Phys. Rev. (1960) 120, 353.
   R.E. Watson, A.J. Freeman, J. Phys. Soc. Japan Suppl. (1962) 17B.1, 40.
2. C. Zener, R.R. Heikes, Rev. Mod. Phys. (1953) 25, 191.
3. M.A. Ruderman, C. Kittel, Phys. Rev. (1954) 96, 99.
4. T. Kasuya, Prog. Theor. Phys. (1956) 16, 45.
5. Key Yosida, Phys. Rev. (1957) 106, 893.
6. P.G. de Gennes, J. Phys. Rad. (1962) 23, 510.

7. P.G. de Gennes, C. R. Acad. Sci. Paris (1958) 247, 1836.

8. A.J. Dekker, J. Appl. Phys. (1965) 36, 906.

9. S.H. Liu, Phys. Rev. (1961) 121, 451.

10. T. Kasuya, Prog. Theor. Phys. (1956) 16, 58.

11. Y.A. Rocher, Adv. in Phys. (1962) 22, 233.

12. Y.A. Rocher, J. Phys. Chem. Sol. (1962) 23, 1621.

13. Y.A. Rocher, Rare Earth Res. IV (1964) 127.

14. E.W. Gorter, U. Enz, J.F. Fast, S. van Houten, J. Smit, J. Appl. Phys. (1963) 34, 1253.

15. F. Holtzberg, T.R. McGuire, S. Methfessel, J.C. Suits, Phys. Rev. Lett. (1964) 13, 18.

16. F. Holtzberg, T.R. McGuire, S. Methfessel, J.C. Suits, J. Appl. Phys. (1964) 35, 1033.

17. J. Grunzweig, M. Kuznietz, J. Appl. Phys. (1968) 39, 905.

18. W.C. Koehler, J. Appl. Phys. (1965) 36, 1078.

C H A P T E R   I I

RUDERMAN AND KITTEL, KASUYA AND YOSIDA INTERACTION.

II-1. Introduction.

The most important interaction that is believed to cause magnetic
long-range order in the rare-earth metals and their metallic conducting
compounds is generally assumed to be an indirect exchange interaction
of localized ionic magnetic moments via the conduction electrons. This
concept is supported by studies of the N.M.R. spectra (Knight-shift[1]),
electron spin resonance [2] and by the fact that the rare-earth oxides
and other ionic rare-earth compounds, having no conduction electrons,
have very low magnetic ordering temperatures.

This indirect type of interaction, that is responsible for the
coupling of nuclear spins, the line broadening in N.M.R. spectra and
for the Knight-shift in metals and metallic compounds, has first been
suggested by Fröhlich and Nabarro [3], and has been worked out in more
detail by Ruderman and Kittel [4]. Zener [5], Kasuya [6], Yosida [7]
and several others [8-13] investigated the analogous interaction via
the conduction electrons of the electronic magnetic moments localized
on the metal atoms.

The interaction of a localized magnetic moment on a metal atom
with the localized magnetic moment on another metal atom can be visua-
lized in the following manner. The scattering of a conduction electron
by a localized magnetic moment $\vec{J}_1$ depends on the interaction $\vec{J}_1 \cdot \vec{s}$,
where $\vec{s}$ is the spin of the conduction electron. A second localized
magnetic moment $\vec{J}_2$ percepts the density of the scattered electron
through the interaction $\vec{J}_2 \cdot \vec{s}$. This process effectuates an interaction
between the two localized magnetic moments $\vec{J}_1$ and $\vec{J}_2$. With an inter-

action of this type the expression obtained for the paramagnetic
Curie-temperature (θ_p) is:

$$\theta_p = \frac{3\pi Z^2 (g-1)^2 J(J+1) \Gamma_s^2 \sum\limits_{m>n} F(2k_F R_{mn})}{4kV^2 \epsilon_F}$$

with: Z is the number of conduction electrons per rare-earth atom,

g is the Landé spectroscopic splitting factor,

J is the magnetic moment of the rare-earth ion,

Γ_s is the exchange interaction between 4f- and conduction electrons,

k is the Boltzmann constant,

ϵ_F is the Fermi energy,

k_F is the Fermi momentum,

R_{mn} is the distance between the rare-earth ion spins.

$$F(2k_F R_{mn}) = \frac{2k_F R_{mn} \cos(2k_F R_{mn}) - \sin(2k_F R_{mn})}{(2k_F R_{mn})^4}$$

II-2. RKKY-theory.

The above-mentioned theory, the so-called Ruderman and Kittel,
Kasuya and Yosida (RKKY) theory, assumes, as given in the approach of
Kittel (14), a nearly free electron model described by Bloch-functions:

$$\phi_{\vec{k}s}(\vec{x}) = e^{i\vec{k}.\vec{x}} u_{\vec{k}s}(\vec{x}) = \phi_{\vec{k}}(\vec{x}) |s> \tag{1}$$

where s is the spin-index and denotes spin-up ($\uparrow$) or spin-down ($\downarrow$) for
s^z.

The perturbation of the conduction electron density created by the
interaction of a localized moment $\vec{J}_n$ at the position $\vec{R}_n$ with a conduction
electron at $\vec{r}_j$ is first calculated. The hamiltonian $\mathcal{H}_1$ for this inter-
action has the form:

$$\mathcal{H}_1 = \Gamma(\vec{r}_j - \vec{R}_n) \; \vec{s}_j \cdot \vec{J}_n \tag{2}$$

17

where $\Gamma(\vec{r}_j - \vec{R}_n)$ is an exchange constant.

For the entire system with many (j) electrons and many (n) localized magnetic moments we have an interaction hamiltonian:

$$\mathcal{H} = \underset{jn}{\Sigma\Sigma} \; \Gamma(\vec{r}_j - \vec{R}_n)\vec{s}_j.\vec{J}_n \tag{3}$$

The electron-field operators are:

$$\psi(\vec{x}) = \underset{\vec{k}s}{\Sigma} \; c_{\vec{k}s} \; \phi_{\vec{k}s}(\vec{x}) \; ; \quad \psi^+(\vec{x}) = \underset{\vec{k}s}{\Sigma} \; c_{\vec{k}s}^+ \; \phi_{\vec{k}s}^*(\vec{x}) \tag{4}$$

where $c_{\vec{k}s}^+$ and $c_{\vec{k}s}$ are the fermion creation and annihilation operators. By using the one electron expectation value: $\int \phi^*(\vec{x})\mathcal{H}\phi(\vec{x}) d^3x$, we obtained the following hamiltonian in second-quantized form:

$$\mathcal{H} = \underset{\substack{\vec{k}\vec{k}' \\ ss'}}{\Sigma} \; \underset{n}{\Sigma} \int d^3x [\phi_{\vec{k}'s'}^*(\vec{x})\Gamma(\vec{x} - \vec{R}_n)\vec{s}.\vec{J}_n \; \phi_{\vec{k}s}(\vec{x})] c_{\vec{k}'s'}^+ \; c_{\vec{k}s} \tag{5}$$

Substituting for $\phi_{\vec{k}s}$ the Bloch functions of (1), we get:

$$\mathcal{H} = \underset{\substack{\vec{k}\vec{k}' \\ ss'}}{\Sigma} \; \underset{n}{\Sigma} \int d^3x [e^{-i\vec{k}'.\vec{x}} u_{\vec{k}'s'}^*(\vec{x})\Gamma(\vec{x} - \vec{R}_n)\vec{s}.\vec{J}_n e^{i\vec{k}.\vec{x}} u_{\vec{k}s}(\vec{x})] c_{\vec{k}'s'}^+ \; c_{\vec{k}s}$$

If we take $\vec{x}' = \vec{x} - \vec{R}_n$, the integral becomes:

$$\int d^3x' [e^{-i\vec{k}'.(\vec{x}'+\vec{R}_n)} u_{\vec{k}'s'}^*(\vec{x}'+\vec{R}_n)\Gamma(\vec{x}')\vec{s}.\vec{J}_n e^{i\vec{k}.(\vec{x}'+\vec{R}_n)} u_{\vec{k}s}(\vec{x}'+\vec{R}_n)]$$

and as $u_{\vec{k}s}(\vec{x}' + \vec{R}_n) = u_{\vec{k}s}(\vec{x}')$, due to the periodicity of the lattice, we may rewrite this as:

$$\int d^3x [e^{-i\vec{k}'.\vec{R}_n} \phi_{\vec{k}'s'}^*(\vec{x})\Gamma(\vec{x})\vec{s}.\vec{J}_n \phi_{\vec{k}s} e^{i\vec{k}.\vec{R}_n}]$$

So we obtain for the hamiltonian:

$$\mathcal{H} = \sum_{\substack{\vec{k}\vec{k}' \\ ss'}} \sum_n e^{i(\vec{k}-\vec{k}')\cdot\vec{R}_n} \int d^3x \phi^*_{\vec{k}'}(\vec{x}) \Gamma(\vec{x}) \phi_{\vec{k}}(\vec{x}) <s'|\vec{s}.\vec{J}_n|s> c^+_{\vec{k}'s'} c_{\vec{k}s} =$$

$$= \sum_{\substack{\vec{k}\vec{k}' \\ ss'}} \sum_n e^{i(\vec{k}-\vec{k}')\vec{R}_n} \Gamma(\vec{k},\vec{k}') <s'|\vec{s}.\vec{J}_n|s> c^+_{\vec{k}'s'} c_{\vec{k}s} \qquad (6)$$

where: $\Gamma(\vec{k},\vec{k}') = \int d^3x \phi^*_{\vec{k}'}(\vec{x}) \Gamma(\vec{x}) \phi_{\vec{k}}(\vec{x})$

With: $\vec{s}.\vec{J}_n = s^z J^z_n + \tfrac{1}{2}s^+ J^-_n + \tfrac{1}{2}s^- J^+_n$ \qquad (7)

where s^+, J^+, s^-, J^- are the raising and lowering operators:

$$\sum_{ss'} <s'|s^z J^z_n|s> c^+_{\vec{k}'s'} c_{\vec{k}s} = \tfrac{1}{2}J^z_n (c^+_{\vec{k}'\uparrow} c_{\vec{k}\uparrow} - c^+_{\vec{k}'\downarrow} c_{\vec{k}\downarrow})$$

$$\tfrac{1}{2}\sum_{ss'} <s'|s^+ J^-_n|s> c^+_{\vec{k}'s'} c_{\vec{k}s} = \tfrac{1}{2}J^-_n c^+_{\vec{k}'\uparrow} c_{\vec{k}\downarrow}$$

$$\tfrac{1}{2}\sum_{ss'} <s'|s^- J^+_n|s> c^+_{\vec{k}'s'} c_{\vec{k}s} = \tfrac{1}{2}J^+_n c^+_{\vec{k}'\downarrow} c_{\vec{k}\uparrow}$$

Consequently

$$\mathcal{H} = \tfrac{1}{2}\sum_{\vec{k}\vec{k}'} \sum_n e^{i(\vec{k}-\vec{k}')\cdot\vec{R}_n} \Gamma(\vec{k},\vec{k}') \{ J^z_n (c^+_{\vec{k}'\uparrow} c_{\vec{k}\uparrow} - c^+_{\vec{k}'\downarrow} c_{\vec{k}\downarrow}) +$$

$$J^+_n c^+_{\vec{k}'\downarrow} c_{\vec{k}\uparrow} + J^-_n c^+_{\vec{k}'\uparrow} c_{\vec{k}\downarrow} \} \qquad (8)$$

The wave function for electrons with spins mainly up is in first order
perturbation theory given by:

$$|\vec{k}\uparrow> = |\vec{k}\uparrow>_0 + \sum_{\vec{k}'s}' |\vec{k}'s>_0 \frac{<\vec{k}'s|\mathcal{H}|\vec{k}\uparrow>}{\varepsilon_k - \varepsilon_{k'}} \qquad (9)$$

where $|\vec{k}\uparrow>_0$ is the unperturbed state with spin up, and the prime in the

19

summation indicates that the state $\vec{k}'s = \vec{k}\uparrow$ is to be excluded from the summation.

If:

$$|\vec{k}s\rangle = V^{-\frac{1}{2}} e^{i\vec{k}.\vec{x}} u_{\vec{k}} |s\rangle \qquad (10)$$

where V is the atomic volume and:

$$\varepsilon_k = \frac{k^2\hbar^2}{2m^*} \qquad (11)$$

is the energy of a nearly free electron in the state $\vec{k}$ and m^* is effective mass of the electron, then we find from the equations 8 and 9:

$$|\vec{k}\uparrow\rangle = |\vec{k}\uparrow\rangle_0 + \frac{m^*}{\hbar^2} \sum_{\vec{k}'}' \frac{\Gamma(\vec{k},\vec{k}')}{k^2 - k'^2} \sum_n e^{i(\vec{k}-\vec{k}').\vec{R}_n} \{J_n^z|\vec{k}\uparrow\rangle + J_n^+|\vec{k}\downarrow\rangle\} \qquad (12)$$

If the $u_{\vec{k}}$ part of the Bloch function is independent of k, and if we take $\Gamma(k,k') = \Gamma_J$ is a constant we may write equation 12 as:

$$|\vec{k}\uparrow\rangle = |\vec{k}\uparrow\rangle_0 + \frac{m^*\Gamma_J}{8\hbar^2\pi^3} P\int d^3k' \frac{e^{i\vec{k}'.\vec{x}}}{k^2 - k'^2} \sum_n \{J_n^z|\uparrow\rangle + J_n^+|\downarrow\rangle\} \qquad (13)$$

The principal value for the integral, which is necessary because of the exclusion of the state $\vec{k}' = \vec{k}$ from the summation over $\vec{k}'$ in the equations 9 and 12, is given by:

$$P\int d^3k' \frac{e^{i\vec{k}'.\vec{x}}}{k^2 - k'^2} = \frac{2\pi^2}{r} \cos kr \qquad (14)$$

thus we have:

$$|\vec{k}\uparrow\rangle = |\vec{k}\uparrow\rangle_0 + \frac{m^*\Gamma_J \cos kr}{4\pi r\hbar^2} \sum_n \{J_n^z|\uparrow\rangle + J_n^+|\downarrow\rangle\} \qquad (15)$$

The electron density corresponding to this wave-function is:

$$\rho(\vec{k}\uparrow) = 1 + \frac{m^*\Gamma_J \cos kr}{2\pi r\hbar^2} \cos kx \sum_n J_n^z \qquad (16)$$

Integrated over the ground state Fermi-sea this gives the total spin-up electron density:

20

$$\rho(\uparrow) = \frac{1}{(2\pi)^3} \int_0^{\vec{k}_F} d^3k \rho(\vec{k}\uparrow) = \frac{k_F^3}{6\pi^2} \{1 - \sum_n \frac{3m^* \Gamma_J J_n^z k_F}{\pi \hbar^2} F(2k_FR)\}$$
(17)

where:

$$F(2k_FR) = \frac{2k_FR\cos 2k_FR - \sin 2k_FR}{(2k_FR)^4}$$
(18)

This is the Ruderman-Kittel function; a graphical representation of this function is given in figure II-1.
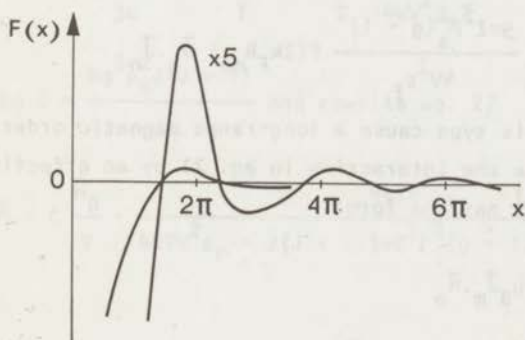
Fig. II-1. *Variation of the Ruderman-Kittel function, $F(x)$, with x (after A. Herpin, Théorie du Magnétisme (ref. 15)).*

We can see that the localized 4f-moments perturb the conduction electron spin in an oscillatory way. In second order this perturbation leads to an interaction between two localized magnetic moments, which is given by the hamiltonian:

$$\mathcal{H}^1 = \sum_{\substack{\vec{k}\vec{k}' \\ ss'}} \frac{\langle \vec{k}s|\mathcal{H}|\vec{k}'s\rangle \langle \vec{k}'s|\mathcal{H}|\vec{k}s\rangle}{\epsilon_k - \epsilon_{k'}}$$
(19)

Using for $\mathcal{H}$ the hamiltonian of eq. 8 and making the same assumptions (eq. 10 and 11, $\Gamma(k,k') = \Gamma_J$, $u_{\vec{k}}$ is independent of $\vec{k}$) we made before, we find:

21

$$\mathcal{H}^1 = \sum_{m>n} \frac{9\pi Z^2 \Gamma_J}{4\varepsilon_F V^2} F(2k_F R_{mn}) \vec{J}_m \cdot \vec{J}_n \tag{20}$$

where: Z is the number of conduction electrons per atom, and V is the atomic volume.

According to the evaluation of de Gennes (15) and Liu (16) the exchange constant Γ_J may be replaced, in the case of a strong spin-orbit coupling, by $(g - 1)\Gamma_s$, where Γ_s is a constant for all rare-earth ions and g is the Landé spectroscopic splitting factor of the ion. Thus the final form for the interaction hamiltonian becomes:

$$\mathcal{H}^1 = \sum_{m>n} \frac{9\pi Z^2 \Gamma_s^2 (g - 1)^2}{4V^2 \varepsilon_F} F(2k_F R_{mn}) \vec{J}_m \cdot \vec{J}_n \tag{21}$$

Interactions of this type cause a long-range magnetic order.

We now replace the interaction in eq. 21 by an effective magnetic field $\vec{H}_e$ so that $\mathcal{H}^1$ has the form:

$$\mathcal{H}^1 = \sum_m g\mu_B \vec{J}_m \cdot \vec{H}_e \tag{22}$$

from eqs. 21 and 22 we may write:

$$\vec{H}_e = \frac{9\pi Z^2 \Gamma_s^2 (g - 1)^2}{4g\mu_B V^2 \varepsilon_F} \sum_{m>n} F(2k_F R_{mn}) \vec{J}_n \tag{23}$$

In the Weiss approximation we may replace each $\vec{J}_n$ by its average $<\vec{J}_n>$, and as all magnetic atoms are identical and equivalent, $<\vec{J}_n>$ is related to the total magnetic moment of the crystal by:

$$\vec{M} = N g\mu_B <\vec{J}_n> \tag{24}$$

From eqs. 23 and 24 we may write:

$$\vec{H}_e = \frac{9\pi Z^2 \Gamma_s^2 (g - 1)^2}{4N g^2 \mu_B^2 V^2 \varepsilon_F} \sum_{m>n} F(2k_F R_{mn}) \vec{M} \tag{25}$$

For a simple paramagnet the magnetization due to a magnetic field $\vec{H}$ is

22

given by:
$$\vec{M} = \frac{Ng^2\mu_B^2 J(J + 1)}{3kT} \vec{H} \tag{26}$$

In the molecular-field model we replace $\vec{H}$ by the sum of the applied field $\vec{H}_0$ and the molecular-field $\vec{H}_e$, hence from eqs. 25 and 26:

$$\vec{M} = \frac{Ng^2\mu_B^2 J(J + 1)}{3kT} (\vec{H}_0 + \vec{H}_e) =$$

$$= \frac{Ng^2\mu_B^2 J(J + 1)}{3k} \frac{\vec{H}_0}{T} + \frac{3\pi Z^2 J(J + 1)\Gamma_s^2 (g - 1)}{4kV^2\varepsilon_F T} \sum_{m>n} F(2k_F R_{mn}) \vec{M} \tag{27}$$

When we take $C = \dfrac{Ng^2\mu_B^2 J(J + 1)}{3k}$ and rewrite eq. 27

$$\vec{M} = C \frac{\vec{H}_0}{T} \cdot \frac{4kTV^2\varepsilon_F}{4kTV^2\varepsilon_F - J(J + 1)3\pi Z^2\Gamma_s^2 (g - 1)\sum\limits_{m>n} F(2k_F R_{mn})}$$

$$= \frac{C}{T - \dfrac{3\pi Z^2 (g - 1)^2 J(J + 1)\Gamma_s^2 \sum\limits_{m>n} F(2k_F R_{mn})}{4kV^2\varepsilon_F}} \vec{H}_0$$

$$= \frac{C}{T - \Theta_p} \vec{H}_0$$

where:
$$\Theta_p = \frac{3\pi Z^2 (g - 1)^2 J(J + 1)\Gamma_s^2 \sum\limits_{m>n} F(2k_F R_{mn})}{4kV^2\varepsilon_F} \tag{28}$$

is the paramagnetic Curie-temperature. From this formula it can be seen that in the case of RKKY-interaction the paramagnetic Curie-temperature, among other things will depend on the conduction electron concentration and on the distances between the magnetic ions.

23

References

1.   A.M. van Diepen, Thesis, Amsterdam (1968).

2.   M. Peter, J. Appl. Phys. (1961) 32, 338.

3.   H. Fröhlich, F.R.N. Nabarro, Proc. Roy. Soc. (1940) A175, 382.

4.   M.A. Ruderman, C. Kittel, Phys. Rev. (1954) 96, 99.

5.   C. Zener, R.R. Heikes, Rev. Mod. Phys. (1953) 25, 191.

6.   T. Kasuya, Prog. Theor. Phys. (1956) 16, 45.

7.   Key Yosida, Phys. Rev. (1957) 106, 893.

8.   S.H. Liu, Phys. Rev. (1961) 121, 451.

9.   A. Blandin, J. Phys. Radium (1959) 20, 160.

10.   T.A. Kaplan, D.H. Lyons, Phys. Rev. (1963) 129, 2072.

11.   Y.A. Rocher, Adv. in Physics (1962) 22, 233.

12.   Y.A. Rocher, J. Phys. Chem. Sol. (1962) 23, 1621.

13.   A.J. Dekker, J. Appl. Phys. (1965) 36, 906.

14.   C. Kittel, Quantum Theory of Solids, J. Wiley & Sons (1963).

15.   A. Herpin, Théorie du Magnétisme, Presses Universitaires de
        France (1968).

CHAPTER III

CRYSTAL CHEMISTRY OF SOME OF THE BINARY AND TERNARY
RARE-EARTH CHALCOGENIDES

III-1.Survey of the rare-earth chalcogenides.

A very extensive survey of the crystal-chemistry of the binary
and ternary rare-earth chalcogenides has been given by Flahaut and
Laruelle (1) and by Flahaut (2). Here only a brief summary of the
phases existing between the rare-earth metals on the one hand and
sulphur, selenium or tellurium on the other hand and also of the mixed
rare-earth metal, alkaline-earth metal chalcogenides will be given.

A schematic representation of the phases existing in the binary
rare-earth chalcogenide series is given in the figures III-1, III-2
and III-3. The phases which are investigated in this thesis are those
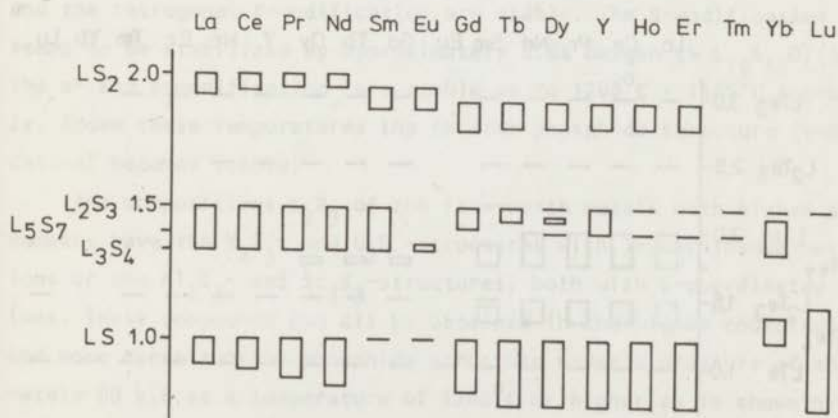
Fig. III-1.*Schematic representation of the phases in the rare-earth
sulphur system (after J. Flahaut and P. Laruelle (ref.1)).*

25

La Ce Pr Nd Sm Eu Gd Tb Dy Y Ho Er Tm Yb Lu

LSe₂ 2.0

L₄Se₇

L₂Se₃ 1.5
L₅Se₇ L₃Se₄
L₅Se₆

LSe 1.0
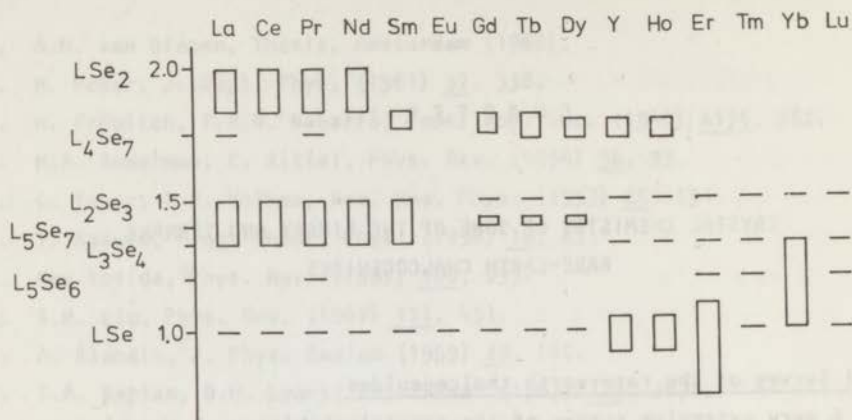
Fig. III-2. *Schematic representation of the phases in the*
rare-earth selenium system (after J. Flahaut and
P. Laruelle (ref. 1)).

La Ce Pr Nd Sm Eu Gd Tb Dy Y Ho Er Tm Yb Lu

LTe₃ 3.0

L₂Te₅ 2.5

LTe₂ 2.0
L₄Te₇
L₂Te₃ 1.5
L₃Te₄
LTe 1.0
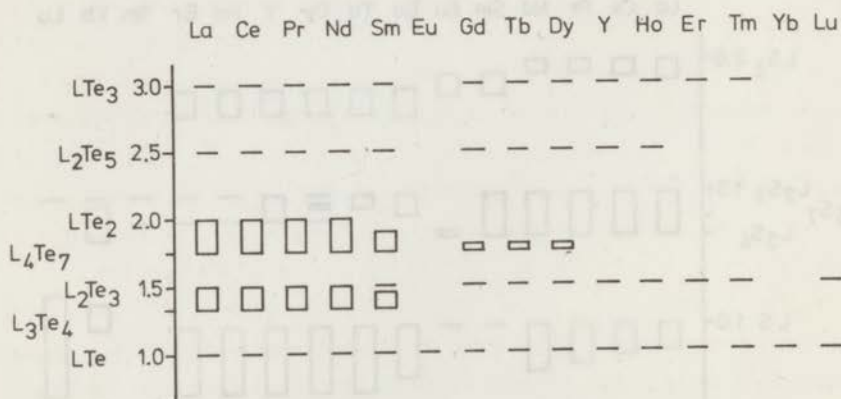
Fig. III-3. *Schematic representation of the phases in the*
rare-earth tellurium system (after J. Flahaut and
P. Laruelle (ref. 1)).

26

with the Th_3P_4-structure, the γ-phase.

This thorium phosphide structure will only exist if the radius of the rare-earth ion with regard to the chalcogen ion is large enough for an eight-coordinated metal ion. This will only be realized with rare-earth metals having a lower atomic number and large radius. For the sulphides the thorium phosphide structure is found in the metal deficient composition, $\square_{1/3}L2_{2/3}S_4$ (equivalent with L_2S_3) from lanthanum up to and including terbium, and for the non-deficient composition, L_3S_4, from lanthanum up to and including europium. Contrary to Flahaut and Laruelle (1) we have also found a phase with the thorium phosphide structure in the dysprosium sulphur system, with a cell-edge of: a = 8.293 Å, but we did not succeed in obtaining this phase pure. In the selenide series we find the thorium phosphide structure from lanthanum up to and including samarium for $\square_{1/3}L2_{2/3}Se_4$ (equivalent with L_2Se_3) as well as for L_3Se_4. For the tellurides $\square_{1/3}L2_{2/3}Te_4$ and L_3Te_4 we find the thorium phosphide structure from lanthanum up to and including neodymium. These facts all agree very well with the assumption that the radius-ratio of cation and anion is the determining factor for the structures in the rare-earth chalcogenides.

In fact the thorium phosphide structure is a high temperature modification. At lower temperatures the orthorhombic α-modification and the tetrogonal β-modification are stable. The β-modification however seems to be stabilized by approximately 0.8% oxygen ($\sim L_{10}S_{14}O$) (3,4,5). The α- and β-modification are stable up to 1200°C - 1400°C approximately. Above these temperatures the thorium phosphide structure (γ-modification) becomes stable.

The compositions L_2X_3 of the rare-earth metals with higher atomnumbers have the Y_2S_3- and U_2S_3-structures with 7-coordinated metal ions or the Al_2O_3- and Sc_2S_3-structures, both with 6-coordinated metal ions. These compounds can all be obtained in the higher coordinated, and more dense thorium phosphide structure under a pressure of approximately 80 k.B at a temperature of 1200°C or higher as is shown by Eatough et al. (6,7).

The ternary chalcogenides of the rare-earth metals with the divalent alkaline-earth metals, of the general formula ML_2X_4 (M = Ca, Sr or

Ba), show a similar behaviour. With the rare-earth metals of lower
atomic number the thorium phosphide structure is obtained; the alkaline-
earth and the rare-earth metal being distributed statistically over the
eight coordinated thorium position. With the rare-earth metals of high-
er atom-number and smaller radius the seven-coordinated ytterbium
selenide structure (8) or the calcium ferrite structure (9) are formed,
the latter with the metal-ions in six- and in eight-coordination.

Chalcogenides of the general formulas: L_2X_3, L_3X_4 and ML_2X_4 crys-
tallizing in the various types of structures are given in table III-1.

III-2.The thorium phosphide structure.

Many of the chalcogenides of the first elements of the rare-earth
metals have as the high temperature crystal structure the eventually
metal-deficient thorium phosphide structure. The thorium phosphide
structure belongs to the very interesting group of cubic crystal struc-
tures with non-intersecting threefold-axes. The space-group is $I\bar{4}3d$
(T_d^6), and the atoms have been placed in the following special positions
(notation after International Tables for X-ray Crystallography).

Th: (12a)

$(0,0,0;\frac{1}{2},\frac{1}{2},\frac{1}{2})$ +   3/8,0,1/4;   1/4,3/8.0;   0,1/4,3/8;

                                    1/8,0,3/4;   3/4,1/8,0;   0,3/4,1/8.

P: (16c)

$(0,0,0;\frac{1}{2},\frac{1}{2},\frac{1}{2})$ +   x,x,x;   1/4+x,1/4+x,1/4+x;

                          1/2+x,1/2-x, $\bar{x}$;   3/4+x,1/4-x,3/4-x;

                             $\bar{x}$,1/2+x,1/2-x;   3/4-x,3/4+x,1/4-x;

                          1/2-x, $\bar{x}$,1/2+x;   1/4-x,3/4-x,3/4+x.

where x equals approximately 1/12.

A projection of the thorium phosphide structure on the (001) plane
is given in figure III-4. A good description of this structure is given
by Yu.A. Kharitonov et al. (10). As a basis for their description these
authors take the distorted octahedron with thorium atoms at the vertices
and a phosphorus atom in its centre. A Penfield projection of this

28

	La	Ce	Pr	Nd	Sm	Gd	Tb	Dy	Ho	Er	Tm	Yb	Lu
	←————————— Th$_3$P$_4$ —————————→							←——— Y$_2$S$_3$ ———→				←— Al$_2$O$_3$ —→	
L$_2$S$_3$	8.731	8.630	8.573	8.527	8.448	8.387	8.334						
	←——— Th$_3$P$_4$ ———→												
L$_3$S$_4$	8.730	8.626	8.575	8.524	8.556								
	←———————————— Th$_3$P$_4$ ————————————→									←—— Yb$_3$S$_4$ ——→			
CaL$_2$S$_4$	8.687	8.615	8.578	8.533	8.472	8.423	8.400	8.376					
	←————— Th$_3$P$_4$ —————→					←——— CaFe$_2$O$_4$ ———→							
SrL$_2$S$_4$	8.790	8.718	8.682	8.649	8.595	8.551							
	←——— Th$_3$P$_4$ ———→				←——— CaFe$_2$O$_4$ ———→								
BaL$_2$S$_4$	8.917	8.864	8.817	8.793									
	←——— Th$_3$P$_4$ ———→				←— U$_2$S$_3$ —→		←——— Sc$_2$S$_3$ ———→						
L$_2$Se$_3$	9.055	8.973	8.927	8.859	8.785								
	←——— Th$_3$P$_4$ ———→							←——— Y$_3$Se$_4$ ———→					
L$_3$Se$_4$	9.055	8.973	8.927	8.859	8.894								
	←———— Th$_3$P$_4$ ————→				←——— CaFe$_2$O$_4$ ———→								
SrL$_2$Se$_4$	9.124	9.060	9.019	8.989	8.931								
	←——— Th$_3$P$_4$ ———→				←——— CaFe$_2$O$_4$ ———→								
BaL$_2$Se$_4$	9.258	9.186	9.150	9.120									

Table III-1. The structures of the rare-earth chalcogenides of the formula: L$_2$X$_3$, L$_3$X$_4$ and ML$_2$X$_4$. For the thorium phosphide-type compounds the cell-edge is given in Å.
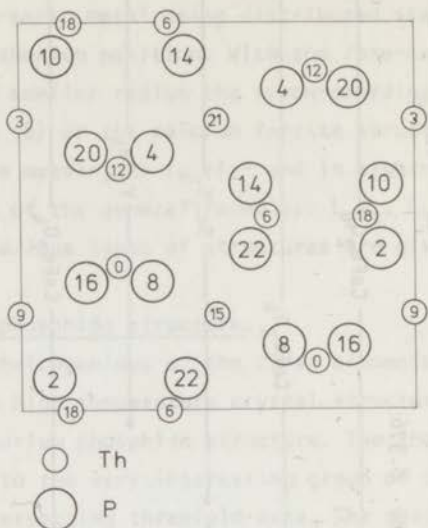
Fig. III-4. *Projection of the cubic thorium phosphide structure*
along a tetragonal axis. Heights of the atoms above
the plane of the paper in 1/24 of the a-axis.

octahedron is given in figure III-5. The distortion can be realized
by rotating the upper plane of a regular octahedron by approximately
22° relative to the basal plane around a threefold axis and a subse-
quent elongation of the octahedron by about 13.4% along the threefold
axis. Along the threefold axes of the cubic cell we have continuous
columns of these octahedra sharing their common equilateral triangles.
In figure III-6 we have indicated one of these columns in the projec-
tion of the structure. Now any octahedron is connected by its two bases
to adjacent octahedra in the same column and by three of its lateral
(and distorted) faces to three octahedra of the other columns corres-
ponding to the other three directions of threefold axes of the cubic
cell. The three remaining and non-shared faces of each octahedron
participate in empty tetrahedra.

This brings us to (distorted) octahedra which share five faces,

30
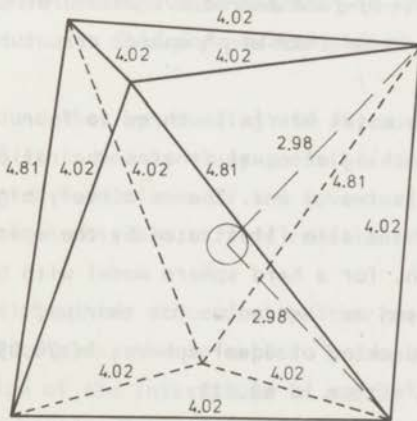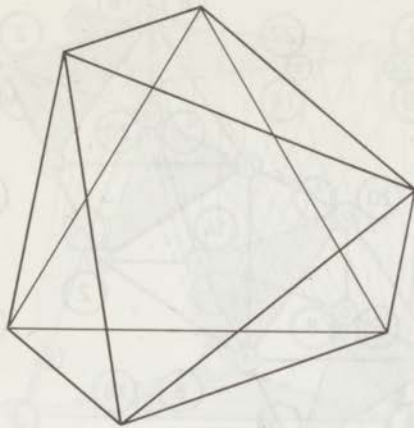
Fig. III-5.*Penfield projection of the distorted thorium
octahedron in the thorium phosphide structure.*

six edges and half of the corners twice and the remaining corners three
times as is indicated in figure III-7. The above-indicated framework
of octahedra is a very dense one, the ratio of the number of tetrahedra
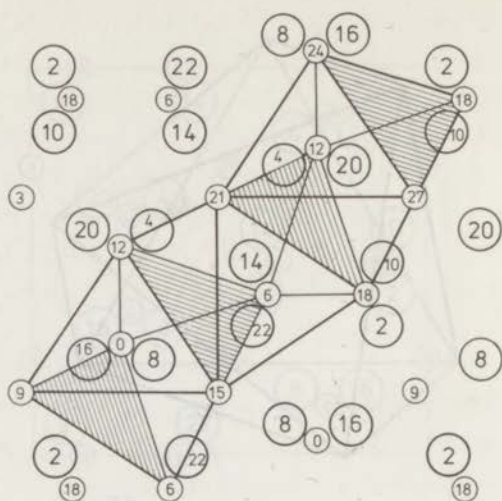
Fig. III-6. *Column of face shared octrahedra along a threefold axis in the thorium phosphide structure.*

and octahedra in this metal matrix is three to four. In structures based on a closest packing of equal spheres the ratio of tetrahedral to octahedral sites is two to one. The relatively high density of this stacking of octahedra is also illustrated by the space-filling of the thorium-lattice which, for a hard sphere model with half of the thorium-thorium distance chosen as the radius for thorium, is 64.3%. For comparison the closest packing of equal spheres is 74.05%, and that of a body-centered cubic lattice is 68.02%.

A quite different description of the thorium phosphide structure is indicated by Loeb (11). For his description of crystal structures Loeb uses the concept of invariant lattice complexes (Niggli (12)). A lattice complex is defined as an arrangement of equivalent points which are related by the symmetry operations of a space-group (13). Such a lattice complex is called invariant when the points have definite and constant coordinates. For the invariant point complexes a nomenclature and a complete taxonomy has been developed by Hermann, Hellner etc.
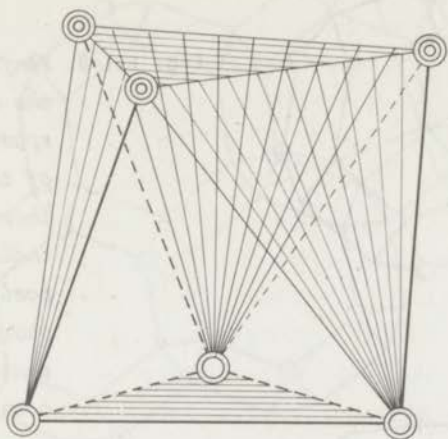
Fig. III-7. *The sharing octahedron of the thorium phosphide struc-
ture.* ◎ *Corner thrice shared* ◯ *Corner twice shared*
━━━ *Edge once shared* ===== *Non-shared edge*
Shaded faces are shared faces.

(14,15,16). Loeb found that by rounding off all coordinates to the near-
est multiple of 1/8 it is nearly always possible to identify a point
complex as a distorted form of one of the invariant lattice complexes.
In this way it is often possible to find relations between crystal
structures.

In the thorium phosphide structure the thorium positions already
occupy an invariant complex, the so-called $^+$S-complex. These positions
are equivalent to 1/8 of the interstices in a body-centered cubic
lattice, or to one quarter of the vanadium positions in V_3Si.

With the parameter of the phosphorus atoms set equal to zero, the
phosphorus positions form an I-complex that is a body-centered cubic
lattice. In the real structure the parameter of the phosphorus positions,
which is approximately 1/12, brings the phosphorus atoms to the centres
of the distorted thorium octahedra, and it brings the coordination of
the thorium from four to eight. As can be seen in the upper part of
figure III-8, which is a projection of the $^+$S-complex, the lower and the
upper plane of the octahedron are rotated by a fixed angle of $21^{\circ}48'$

33
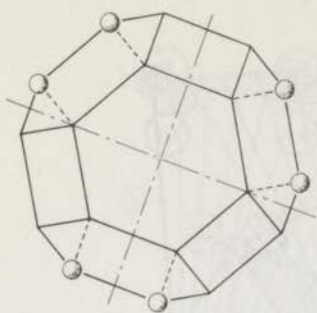
Fig. III-8. *Penfield projection of the stacking of two space-filling polyhedra of the bcc-lattice. The thorium positions are indicated, the idealized position of the phosphorus atoms is in the centres of the cubo-octahedra.*
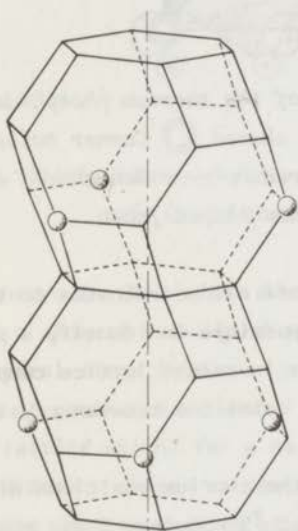
relative to a regular octahedron. The lower part of figure III-8 gives the Penfield projection of the stacking of two space-filling polyhedra of the bcc-lattice (cubo-octahedra, Gorter (17)), with the idealized thorium and phosphorus positions. The stacking of these cubo-octahedra in the different directions of the threefold axes is given in figure III-9.

III-3. Ordering on the cation sites in the thorium phosphide structure.

F.L. Carter (18-21) has studied recently the possibility of cationic charge ordering and vacancy ordering in the thorium phosphide

34
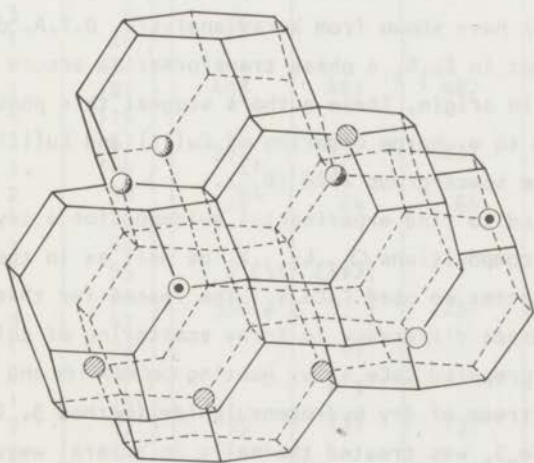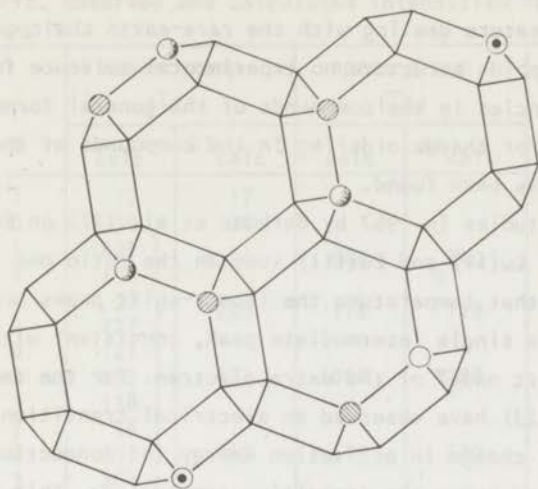
Fig. III-9.*The stacking of the cubo-octahedra of the idealized thorium-phosphide structure in different directions of the threefold axes.*

⬲ *Height above the plane of the paper is $1/12\sqrt{3}$ of the a-axis.*
○ *Height above the plane of the paper is $1/6\sqrt{3}$ of the a-axis.*
◉ *Height above the plane of the paper is $1/4\sqrt{3}$ of the a-axis.*
◑ *Height above the plane of the paper is $1/3\sqrt{3}$ of the a-axis.*
◍ *Height above the plane of the paper is $5/12\sqrt{3}$ of the a-axis.*

related structures.

In the literature dealing with the rare-earth chalcogenides having the thorium phosphide structure no experimental evidence for the ordering of vacancies in the compounds of the general formula: $\square_{1/3}L2_{2/3}X_4$ or for charge ordering in the compounds of the general formula: ML_2X_4 has been found.

Mössbauer studies in 1967 by Berkooz et al. (22) on Eu_3S_4 show the existence of Eu(II) and Eu(III) ions in the ratio one to two below 210 K but above that temperature the isomer-shift peaks broaden and then merge into a single intermediate peak, consistent with a hopping electron transport model of the extra electron. For the same compound Bransky et al. (23) have observed an electrical transition near 175 K, due to an abrupt change in activation energy for conduction from 0.16 eV to 0.21 eV below the transition temperature. This is in reasonable agreement with 0.24 eV obtained by Berkooz et al. More recently Davis et al. (24) have shown from X-ray analysis, D.T.A. data and magnetic data that in Eu_3S_4 a phase transformation occurs at 168 K which is non-magnetic in origin. These authors suggest this phase transformation to be due to a charge ordering of Eu(II) and Eu(III) in a tetragonal cell of the space-group $I\bar{4}2d$ (D_{2d}^{12}).

We have tried to find experimental evidence for a crystallographic ordering in the compositions $\square_{1/3}L2_{2/3}X_4$ as well as in the compositions ML_2X_4. For the latter we used $CaCe_2S_4$. The reason for this choice was the relatively great difference in X-ray scattering of calcium and cerium ions. We prepared $CaCe_2S_4$ by heating cericoxide and calciumcarbonate in a stream of dry hydrogensulphide (method 3, Chapter V-1). The obtained $CaCe_2S_4$ was treated thermally in several ways in order to obtain crystallographic ordering. After this treatment X-ray powderdiffraction data were collected. All different treated materials gave the same results. In table III-2 we have collected the observed and calculated diffraction data for the thorium phosphide structure with calcium and cerium statistically distributed over the position 12a of the space-group $I\bar{4}3d$ (T_d^6) and for the "zellengleiche" sub-group $I\bar{4}2d$ (D_{2d}^{12}) with the calcium-ions and the cerium-ions on the positions 4a and 8d respectively. The calculated X-ray diffraction data were

36

Table III-2. Observed and calculated intensities for $CaCe_2S_4$.

h k l	space-group $I\bar{4}2d$ I_{calc}	ΣI_{calc}	space-group $I\bar{4}3d$ I_{calc}	ΣI_{calc}	I_{obs}
1 0 1	17	17			n.o.
2 0 0	30	30			n.o.
2 1 1	1000	1286	840	840	714
1 1 2	286				
2 2 0	33	250	118	118	128
2 0 2	227				
3 1 0	121				
3 0 1	212	471	1000	1000	1000
1 0 3	138				
3 2 1	48				
3 1 2	137	469	519	519	655
2 1 3	284				
4 0 0	5	28	12	12	39
0 0 4	23				
3 0 3	0	26			n.o.
4 1 1	26				
4 2 0	112				
4 0 2	181	408	407	407	321
2 0 4	115				
3 3 2	57	201	237	237	212
3 2 3	144				
4 2 2	99	124	64	64	78
2 2 4	25				
4 3 1	68				
4 1 3	95		163		
3 1 4	71	350		232	296
5 1 0	42				
5 0 1	23		69		
1 0 5	51				
5 2 1	14				
5 1 2	17	55	131	131	131
2 1 5	24				
4 4 0	15	19	14	14	13
4 0 4	4				
4 3 3	7				
5 3 0	0	13	5	5	n.o.
5 0 3	3				
3 0 5	3				
4 2 4	17	19			n.o.
6 0 0	2				
5 3 2	42		175		
5 2 3	41				
3 2 5	32	239		283	287
6 1 1	98		108		
1 1 6	26				

obtained with the aid of a computer program written by Dr. H.M. Rietveld
of the R.C.N. Petten, the Netherlands. The agreement of observed and
calculated data is fairly good for the model with the calcium and cerium
ions distributed statistically over the position 12a of the space-group
$I\bar{4}3d$.

For $\square_{1/3}Pr2_{2/3}S_4$ and for $\square_{1/3}Nd2_{2/3}S_4$ the observed intensities are
also in good agreement with those calculated for a model with the
vacancies statistically distributed over the cation positions in the
thorium phosphide structure, as can be seen in table III-3.

III-4. Parameter variations in rare-earth chalcogenides with the thorium phosphide structure.

In the rare-earth chalcogenides with the thorium phosphide struc-
ture it will be possible to vary both the conduction electron concen-
tration and the cell edge almost independently. This is the reason why
these compounds seem to form an excellent subject to study the indirect
magnetic interactions of the RKKY type. For instance going from Ce_2S_3
fitting with the crystal structure $\square_{1/3}Ce2_{2/3}S_4$ (where $\square$ denotes a
cation vacancy)   to Ce_3S_4, the interatomic distances will hardly vary
($\square_{1/3}Ce2_{2/3}S_4$: a = 8.630 ± 5 Å, Ce_3S_4: a = 8.625 ± 5 Å). The number
of conduction electrons, however, assuming an ionic model with trivalent
cerium and divalent sulphur, will vary from zero to one per formula
unit, which is reflected in the electrical resistance and other
physical properties (figure III-10 ($\square_{1/3}Ce2_{2/3}S_4$: $\rho > 1000 \times 10^{-6}$ Ωcm,
Ce_3S_4: $\rho = 0.58 \times 10^{-6}$ Ωcm)). From $BaCe_2S_4$ (a = 8.864 Å) to Ce_3S_4 both
conduction electron concentration and interatomic distance vary.

As the compounds with the thorium phosphide structure form a com-
plete homogeneous system, it will be possible to prepare compositions
in the quaternary system between: $\square_{1/3}L2_{2/3}X_4$, L_3X_4, AL_2X_4 and BL_2X_4
of the general formula:

$$\theta_{1-(x+y+z)} \square_{1/3x} A_y B_z L_{3-(1/3x+y+z)} X_4$$
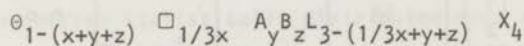
h k l	I_{calc}	I_{obs}	I_{calc}	I_{obs}
	Pr$_2$S$_3$		Nd$_2$S$_3$	
2 1 1	1000	v.s.	1000	v.s.
2 2 0	140	m.	140	m.
3 1 0	997	v.s.	996	v.s.
2 2 2	4	n.o.	4	n.o.
3 2 1	504	v.s.	502	v.s.
4 0 0	16	v.w.	16	v.w.
4 1 1	3 }	n.o.	3 }	n.o.
3 3 0	0 }		0 }	
4 2 0	445	v.s.	447	v.s.
3 3 2	256	s.	255	s.
4 2 2	70	w.	69	w.
5 1 0	86 }	s.	86 }	s.
4 3 1	183 }		182 }	
5 2 1	145	m.	144	m.
4 4 0	16	v.w.	16	v.w.
5 3 0	4 }	n.o.	4 }	n.o.
4 333	1 }		1 }	
6 0 0	0 }	n.o.	0 }	n.o.
4 4 2	3 }		3 }	
6 1 1	113 }	s.	112 }	s.
5 3 2	189 }		188 }	
6 2 0	57	w.	57	w.
5 4 1	150	m.	149	m.
6 2 2	1	n.o.	1	n.o.
6 3 1	62	w.	61	w.
4 4 4	70	w.	70	w.
5 4 3	7 }	n.o.	7 }	n.o.
5 5 0	0 }		0 }	
7 1 0	2 }		2 }	
6 4 0	77	w.	77	w.
7 2 1	96 }	m.	95 }	m.
6 3 3	48 }		48 }	
5 5 2	47 }		47 }	
6 4 2	53	w.	53	w.
7 3 0	20	v.w.	20	v.w.

Table III-3. Observed and calculated intensities for Pr$_2$S$_3$ and
Nd$_2$S$_3$ for a model having the thorium phosphide structure with
statistically distributed metal vacancies.
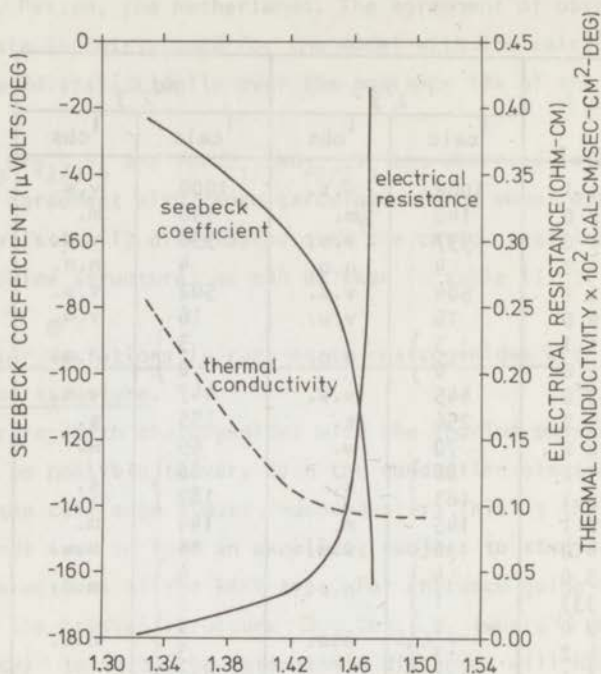
Fig. III-10.*Electrical resistance, Seebeck coefficient and thermal conductivity of CeS$_x$ (1.33 < x < 1.50) (after J.C. Danko et al. (ref. 24)).*

where: $\ominus$ is an electron

      $\square$ is a cation vacancy

      A   is a divalent alkaline-earth cation

      B   is a divalent alkaline-earth cation

      X   is a chalcogen anion

      $x = 0 \rightarrow 1$; $y = 0 \rightarrow 1$; $z = 0 \rightarrow 1$; $x + y \times z \leq 1$.

With compositions of this general formula it is possible to vary the interatomic distances and the number of conduction electrons almost independently.

Due to the distribution of the thorium phosphide type structure

over the rare-earth chalcogen series we were restricted to the elements
La, Ce, Pr, Nd, Pm and Sm. Our only possible choice was the elements
praseodymium and neodymium. The reasons for these limitations are: for
La(III), the lack of magnetic moment; for Ce(III) the large extent of
the 4f-orbital so that direct- and superexchange play a larger role
here; for Pm(III) the radioactivity of this element and for Sm(III) the
small spacing of the J-multiplet levels relative to kT. So we investi-
gated the systems:

$$\square_{1/3}Pr2_{2/3}S_4 \quad - \quad Pr_3S_4 \quad - \quad CaPr_2S_4 \quad - \quad BaPr_2S_4$$

$$\square_{1/3}Pr2_{2/3}Se_4 \quad - \quad Pr_3Se_4 \quad - \quad SrPr_2Se_4 \quad - \quad BaPr_2Se_4$$

$$\square_{1/3}Nd2_{2/3}S_4 \quad - \quad Nd_3S_4 \quad - \quad CaNd_2S_4 \quad - \quad BaNd_2S_4$$

$$\square_{1/3}Nd2_{2/3}Se_4 \quad - \quad Nd_3Se_4 \quad - \quad SrNd_2Se_4 \quad - \quad BaNd_2Se_4$$
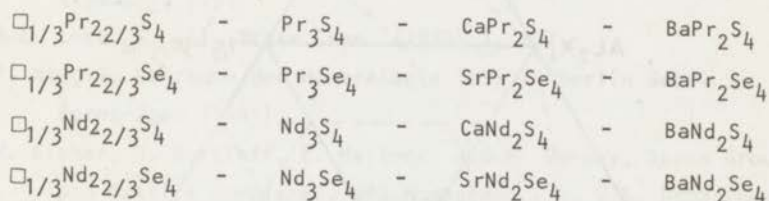
In figure III-11 is indicated how we selected among all possible
compositions in these quaternary systems, the compositions to be measured.
This figure gives the four equilateral triangles forming the faces
of a regular tetrahedron, which represents a quaternary system. First
we limited ourselves to the isoelectronic planes with 0, 1/3, 2/3 and
1 electron per formula unit represented in figure III-11 by the dash-
dot lines. Then starting with the binary compositions on these planes
we prepared compositions with equal cell-edge on the other planes. This
is indicated by the dashed lines in figure III-11. In this way it is
possible, providing Vegart's law will hold, to obtain series of com-
positions with equal cell-edge and varying electron concentration.
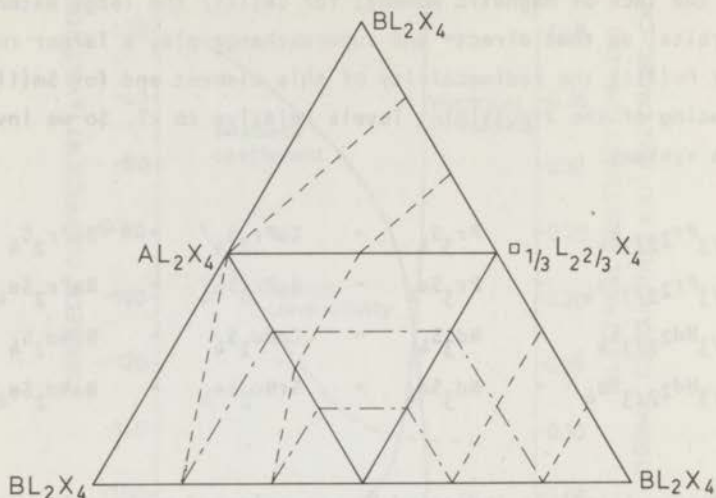
Fig. III-11. *Quaternary system between:* $\square_{0.333}L_{2.667}X_4$, L_3X_4,
AL_2X_4 *and* BL_2X_4. *General formula of the compositions*
in this system is:

$$\Theta_{1-(x+y+z)}\square_{0.333x}A_xB_yL_{3-(0.333x+y+z)}X_4.$$

———: *Lines indicating planes of equal interatomic*
distances.

—·—·—·—: *Lines indicating planes of equal electron*
concentration.

References

1. J. Flahaut, P. Laruelle, Prog. Sci. Technol. Rare Earths 3
       p. 149 ff.
2. J. Flahaut, Prog. Sci. Technol. Rare Earths 3 p. 209 ff.
3. D. Carré, P. Laruelle, P. Besançon, C.R. Acad. Sci. Paris (1970)
       270C, 53.

4.   P. Besançon, C.R. Acad. Sci. Paris (1968) 267C, 1130.

5.   P. Besançon, D. Carré, M. Guittard, J. Flahaut, C.R. Acad. Sci.
          Paris (1970) 271C, 678.

6.   N.L. Eatough, A.W. Webb, H.T. Hall, Inorg. Chem. (1969) 8, 2069.

7.   N.L. Eatough, H.T. Hall, Inorg. Chem. (1970) 9, 417.

8.   C. Souleau, M. Guittard, P. Laruelle, Bull. Soc. Chim. (1969) 9.

9.   B.F. Decker, J.S. Kasper, Acta Cryst. (1957) 10, 332.

10. Yu.A. Kharitonov, N.L. Smirnova, N.V. Belov, J. Struct. Chem.
          (1966) 1, 825.

11. A.L. Loeb, J. Sol. State Chem. (1970) 1, 237.

12. P. Niggli, Lehrbuch der Mineralogie Teil 1. Berlin Gebr.
          Bornträger (1941).

13. W. Fisher, H. Burzlaff, E. Hellner, J.D.H. Donnay, Space Groups
          and Lattice Complexes, NBS Monograph 134, U.S. Department
          of Commerce (1973).

14. C. Hermann, Z. Kristallogr. (1960) 113, 178.

15. E. Hellner, Acta Cryst. (1965) 19, 703.

16. H. Burzlaff, W. Fisher, E. Hellner, Acta Cryst. (1968) A24, 57.

17. E.W. Gorter, J. Sol. State Chem. (1970) 1, 279.

18. F.L. Carter, Rare Earth Res. IV (1964) p. 495.

19. F.L. Carter, Metallurgy of Semicond. Mat., Interscience, New
          York (1961) p. 245.

20. F.L. Carter, Proc. of 8th R.E. Conference (1970) p. 412.

21. F.L. Carter, J. Sol. State Chem. (1970) 5, 300.

22. O. Berkooz, M. Malamud, S. Shtrikman, Sol. State Commun. (1968)
          6, 185.

23. I. Bransky, N.M. Tallan, A.Z. Hed, J. Appl. Phys. (1970) 41, 1787.

24. H.H. Davis, I. Bransky, N.M. Tallan, J. Less-Common Met. (1970)
          22, 193.

25. J.C. Danko, A. Biancheria, F.L. Carter, R.R. Ferber, A.E. Fein,
          H.M. Ferrari, W.D. Johnston, G.R. Kilp, G.L. Thomas,
          Westinghouse Electric Corp., Atomic Power Dept. Rep. -
          1162 (1959).

43

CHAPTER IV

MAGNETIC MEASUREMENTS

IV-1.Introduction

In the range 2 K to 100 K magnetic measurements were carried out by means of a Princeton Applied Research (P.A.R.) Parallel Field Vibrating Sample Magnetometer Model 150. These measurements were performed in magnetic fields up to 56 kOe produced by a superconducting Nb-Zr coil. Details of the apparatus were described by H.T. Witteveen (1). In the temperature range 80 K to 1200 K we used for the magnetic measurements an automatic Faraday-balance which will be described in IV-2.

We analyzed the magnetic behaviour of our compounds in the paramagnetic region with the Curie-Weiss law:

$$X_m = [C/(T - \Theta)] - A$$

where: X_m is the magnetic susceptibility in $cm^3 mole^{-1}$.

C is the Curie constant in $cm^3 degree\ mole^{-1}$.

Θ is the asymptotic Curie temperature in K.

T is the temperature in K.

A is a temperature independent contribution in $cm^3 mole^{-1}$.

The Curie-Weiss law can generally be used for samples with localized moments. In that case the temperature independent correction, A, is a diamagnetic one due to the core electrons. For such a diamagnetic term we corrected our experimental data, using the diamagnetic susceptibilities per mole as tabulated by Selwood (2). If also collective

44

electrons are present temperature independent Pauli paramagnetism must also be taken into account. When however the multiplet intervals are comparable to kT, as is the case with Eu(III) and Sm(III), the simple Curie-Weiss law will no longer hold and a different dependency of χ_m from T will be expected.

Values for the Curie-Weiss parameters C, Θ and A were calculated from the observed molar susceptibilities and temperatures, on an IBM 360/65 computer, with the aid of a least squares approximation program written by Rietveld (R.C.N. Petten, the Netherlands). From the relation:

$$\mu_{eff} = (\frac{3kC}{N\mu_B^2})^{\frac{1}{2}}$$

where:

μ_{eff} is the effective magnetic moment

k   is the Boltzmann constant

N   is Avogadro's number

μ_B is the Bohr magneton

the effective magnetic moment can be calculated.

IV-2. The automatic Faraday balance.

Measurements of the magnetic susceptibility in the temperature range from 80 K to 1200 K were performed by using the Faraday method (2,3). The general set-up of the apparatus we used is a modification of the apparatus described by J.W. Roelofsen (4).

The Faraday method, for measuring magnetic susceptibilities, is a force method based on the fact that if a sample is placed in an inhomogeneous magnetic field H_x in the x-direction ($H_y = H_z = 0$) the force, F_z, in the z-direction, exerted on the sample is given by:

$$F_z = (m\chi_s + \chi_v)H_x \frac{\partial H_x}{\partial z} \text{ dynes}$$

where:

F_z is the force exerted on the sample in dynes

m   is the mass of the sample in grams

45

χ_s is the magnetic susceptibility of the sample in $cm^3 g^{-1}$

χ_v is the magnetic susceptibility of the sample holder in cm^3

H_x is the magnetic field in the x-direction in Oe

$\partial H_x/\partial z$ is the magnetic field gradient in Oe cm^{-1}.

The geometry of our equipment (figure IV-1) has been chosen in such a manner as to make the field gradient (z-direction) vertical. Now the force exerted on the sample, which for a magnetically isotropic sample also will be vertical, can be measured with a microbalance as if it was a difference in weight. The balance we use is an automatic compensated balance, Ugine Eyraud type B60, which can be evacuated. At one side of the balance beam a silica wire with a silica sample holder is suspended, at the other side is suspended a permanent bar-magnet in the
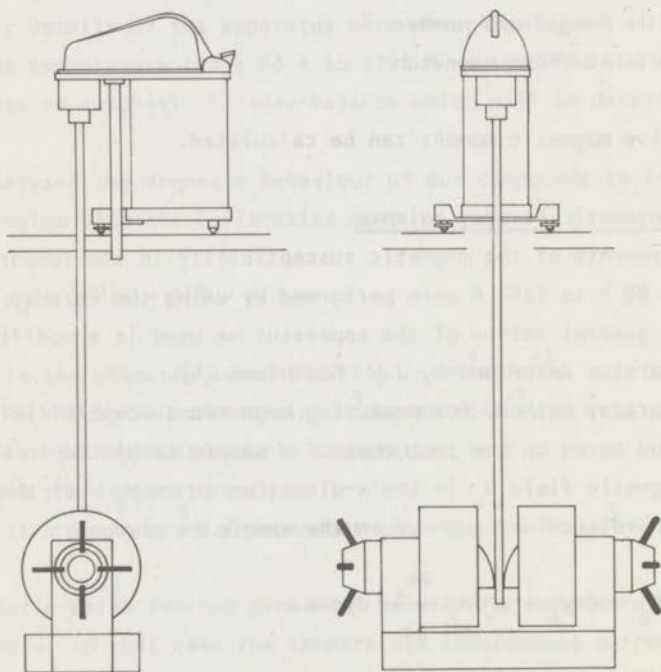
Fig. IV-1. *Faraday equipment.*

46

field of a solenoide. The force on the sample is automatically compen-
sated by a current through the solenoide. When the balance beam is out
of its equilibrium position the illumination of a photo-resistor is
changed. An amplifier system tries to keep the illumination of the
photo-resistor on a fixed value and brings back the balance beam in
its equilibrium position by changing the current through the solenoide.
The change of the current through the solenoide, which is measured over
a potentiometer as a change in voltage, is directly proportional to
the change in the force exerted on the sample. As this compensation
system is sensitive to magnetic fields in the neighbourhood, e.g. to
the leakage field of the electromagnet we use for our measurements,
the balance is screened magnetically by inserting a weak-iron sheet
between the electromagnet and the balance. The small influence of the
leakage field that remains after this shielding is involved in the
correction for the empty sample holder.

The output voltage of the balance is transmitted to a digital
millivolt meter (Solartron type LM1420) and via a signal reducer, which
reduces the signal with approximately 0%, 25%, 50% or 75% of the origi-
nal signal, also to a 2.5 mV Honeywell chart recorder, in order to
check the stability of the balance. The sensitivity of the balance, in
the way we generally use it, is 650 mV $gram^{-1}$. The stability of the
balance is 5×10^{-6} gram.

The sample holder is surrounded by a tube (figure IV-2) around
which a non-inductive wound coil as heating element. The temperature
of the sample is measured with a chromel-alumel thermocouple for the
measurements in the low temperature region (80 K to 300 K) and with a
Pt/Pt - 13% Rh thermocouple for the high temperature region (300 K to
1200 K). The cold junction of the thermocouples was at 0°C and the
electromotive force was also measured with the Solartron LM1420 digital
millivoltmeter. The thermocouples were calibrated with a platinum re-
sistance thermometer (H. Drijfhout en zoon; type WP-KE-33, DIN-43760).

The magnetic field is generated by an electromagnet provided with
constant force pole-caps. For the low temperature region we use a Dings
electromagnet type GM-1 and for the high temperature region we use a
Brucker electromagnet type B-E 10 S4. As power supply we use a

47
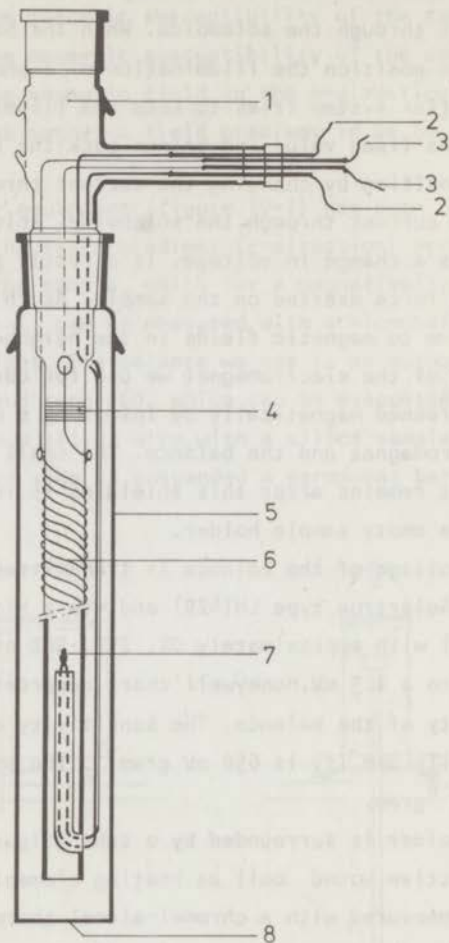
Fig. IV-2. *Lower part of the sample device.*

1.   *Sample tube.*
2.   *Thermocouple leads.*
3.   *Furnace leads.*
4.   *Glass-metal joint.*
5.   *Outer tube.*
6.   *Bifilary wound furnace.*
7.   *Thermocouple.*
8.   *Window.*

specially designed rectifier of high stability built and developed by
- Jesse Electro Apparaten en Transformatoren Fabriek B.V. -.

The magnetic susceptibility per mole of a compound is computed
by using the following formula:

$$X_m = [U_i - V_i] \; C_i \frac{M}{G}$$

where:

X_m is the magnetic susceptibility of the sample in cm^3mole^{-1}.

U_i is proportional to the force experienced on the sample and
the sample holder by the magnetic field i.

V_i is proportional to the force experienced on the empty sample
holder by the magnetic field i.

C_i is a constant whose value is proportional to the product of
the field strength and the field gradient of the magnetic
field i.

M is the molecular weight of the sample.

G is the weight of the sample in grams.

The values of U_i, V_i and C_i depend on the strength of the magnetic field.
The values of C_i for the five fixed values we generally use for the
current through the electromagnet are determined by a relative method
which was based on the magnetic data of mercurytetraisothiocyanato-
cobaltate, $Hg[Co(CNS)_4]$ (5,6). In order to check this way of calibra-
tion and in order to check our temperature measurements we used a sample
of gadolinium sesquioxide. We measured several times samples of Gd_2O_3
(cacermet 99.999%) which were heated in air at 800°C to remove traces
of water. The magnetic data of these samples obeyed the Curie-Weiss
law with:

$$X_{at} = \frac{C_{at}}{T - \theta} = \frac{7.77}{T + 16.3}$$

This result is in good agreement with the results of Arajs and Colvin
(7) who found the values $C_{at} = 7.80 \; cm^3at^{-1}$ and $\theta = -17$ K in the tem-
perature range between 300 K and 1500 K.

The Faraday equipments are completely automized. A schematic
diagram of the overall measuring system is shown in figure IV-3. The

49
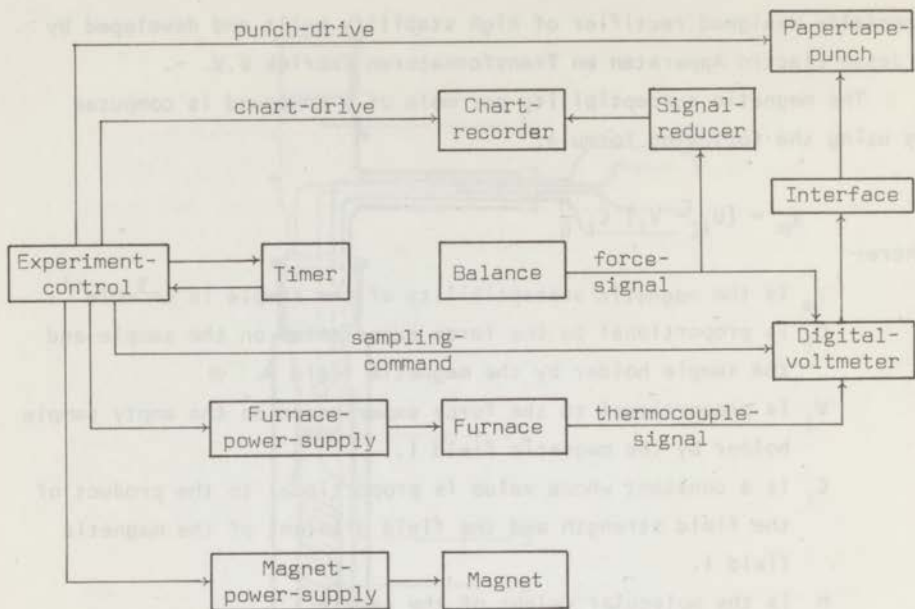
Fig. IV-3. *Block diagram of the automatic magnetic Faraday system.*

experiment control unit consists of a programmed switch which controls
a program cycle consisting of eight measurements: one force measure-
ment at zero field, followed by five force measurements at five dif-
ferent values of the magnetic field, another force measurement at zero
field and finally one temperature measurement. For each temperature
this cycle is repeated four times. The results of these 32 measurements
are punched on a paper-tape. As these four cycles have been performed
the temperature is altered and after temperature equilibrium has been
reached a new set of four measuring cycles is started. So we obtain
with the aid of a computer program, for each temperature four values
of the magnetic susceptibility at five different values of the mag-
netic field.

References

1. H.T. Witteveen, Thesis, Leiden (1973).
2. P.W. Selwood, Magnetochemistry, Interscience Publishers Inc., New York (1956) 2nd ed.
3. M. Faraday, Experimental Research, Taylor and Francis, London (1855) Vol. III.
4. J.W. Roelofsen, Thesis, Leiden (1967).
5. B.N. Figgis, R.S. Nyholm, J. Chem. Soc. (1958) 4190.
6. B.N. Figgis, R.S. Nyholm, J. Chem. Soc. (1959) 338.
7. S. Arajs, R.V. Colvin, J. Appl. Phys. $\underline{33}$ (1962) 2517.

51

C H A P T E R V

EXPERIMENTAL DATA AND RESULTS

V-1. Preparation of the samples.

The most general techniques for preparing sulphides and selenides of the rare earth metals are:

1:    Direct reaction between the elements.

2:    Reaction of powdered metal with dry hydrogen sulphide or hydrogen selenide.

3:    Reaction of metal oxides, metal carbonates or mixtures thereof with hydrogen sulphide, hydrogen selenide or carbon disulphide.

4:    Reaction of rare earth metal compounds with dry hydrogen sulphide or hydrogen selenide.

5:    Reduction of sulphates, selenates, sulphites or selenites with dry hydrogen gas.

6:    Solid state reaction of powdered and compressed mixtures of the products obtained by one or more of the above-mentioned methods.

ad.1: The desired quantities of the rare earth metal and sulphur or selenium were put in a degassed silica tube, which was evacuated to a pressure of about 10^{-3} - 10^{-4} torr and sealed. The tube was heated in an electrical furnace, first at 500 ^{o}C to prevent any attack of the silica by the metal and in order to maintain the sulphur or selenium vapour pressure low. After all sulphur or selenium vapour had disappeared, the temperature was raised to 1100 ^{o}C for a week. After this week the samples were cooled quickly (quenched) to room temperature. If X-ray diffraction showed that the reaction had not been completed or that one of the low-temperature phases had been formed, the samples

were powdered in an agate mortar and subsequently compressed into a
cylinder. This cylinder was heated in a thick-walled tantalum crucible
placed in a sealed evacuated (to a pressure smaller than 10^{-5} torr)
silica tube at 1400 $^{\circ}$C, by means of a high frequent induction furnace.
With X-ray fluorescence no tantalum could be detected in the samples
after this treatment.

ad.2: This method of preparation was not used in our investigations.
      Because this method only allows us to obtain the sesquisulphides
of the rare earth metals, as is the case with the third method, and
because some of the rare earth metals are pyrophoric and not easy to
handle, we preferred to use the third method.

ad.3: The rare earth oxides were placed in a graphite crucible (Schunck
      and Ebe, quality FE 49). This crucible was surrounded by a layer of
non-conducting graphite felt (Schunck and Ebe) and by a cylindrically
shaped graphite radiation shield with vertical slits to avoid energy
pick-up from the H.F. field. This whole ensemble was placed in a silica
tube and heated in a stream of dry hydrogen sulphide at a temperature
of 1300 - 1500 $^{\circ}$C by means of a high frequent induction furnace (figure
V-1). The products obtained by this method are in most cases the rare
earth sesquisulphides, which lie on the sulphur-rich side of the thorium
phosphide type phase extension area, as shown by Klemm et al. (1).
Only in the case of europium, Eu_3S_4 or even EuS or a mixture thereof
is formed according to the circumstances of the reaction. We employed
this method with hydrogen sulphide only.

ad.4: The reaction between hydrogen sulphide or hydrogen selenide and the
      salts of the rare earth metals shows the same advantages and dis-
advantages as the former method. Consequently we did not use this reac-
tion for preparing our compositions.

ad.5: The reduction of sulphates, selenates, sulphites or selenites with
      dry hydrogen has many disadvantages. For instance, it is very hard
to avoid the chalcogen element being lost due to the reverse reaction

53
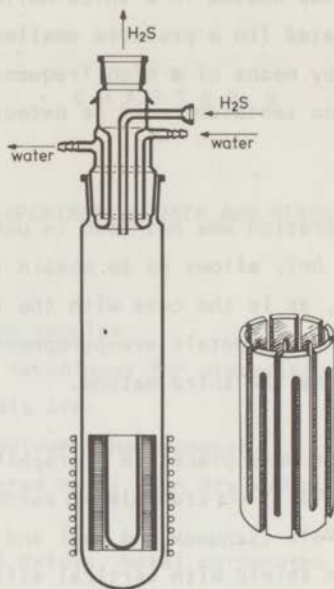
Fig. V-1. *Equipment for the preparation of rare earth sulphides.*
The cylindrically shaped radiation shield is given in
detail.

of the water formed during the reaction, with the sulphide or selenide
(2). We only used this method to obtain the selenides of barium and
strontium (2), which we used to prepare ternary strontium and barium
rare earth selenides according to the sixth method.

ad.6:To obtain the intermediate phases between those prepared by one
of the methods 1, 3 and 5, we compressed appropriate amounts of
powdered specimen obtained by said methods into cylinders. These cylin-
ders were heated in a thick-walled tantalum crucible placed in a sealed
and evacuated (to a pressure of about 10^{-5} - 10^{-6} torr) silica tube by
means of a high frequent induction furnace at 1400 °C. X-ray fluorescence
showed that after this treatment no trace of tantalum was present in the
samples.

The rare earth metals used were powders or chips of high purity grade, better than 99.9% (Cacermet, Elcomat). By X-ray fluorescence no trace of other than the assumed rare earth metals could be detected.

The rare earth oxides had a claimed purity of 99.9% (Cacermet, Elcomat). By means of X-ray fluorescence no rare-earth metals except the assumed ones could be detected.

The sulphur and the selenium used, had both claimed purities of 99.999% (Fluka A.G.), the carbonates of calcium strontium and barium all had claimed purities of 99.9% (Merck A.G.), the selenates of strontium and barium had a purity better than 99.9% (K & K). The hydrogen sulphide we used had a purity better than 99.5% (Loosco). Prior to use we dried the hydrogen sulphide over phosphorus pentoxide.

V-2. Characterization of the samples.

X-ray diffraction analysis was carried out by means of a Guinier-de Wolf camera, and by means of a Philips powder diffractometer, type PW 1025/25, equipped with a graphite monochromator. In both cases we used Cu K-α radiation (λ = 1.5418 Å). In the powder diffractometer all samples were examined with the reflection method. In view of the possible influence of preferred orientation of the crystallites due to the flat sample holder of the diffractometer on the intensities of the diffraction lines, some samples were also investigated with the transmission method. As no significant differences in the intensities obtained by these two methods could be detected the influence of preferred orientation of the crystallites on the intensities may be neglected.

The cell dimensions and the intensities were calculated on an I.B.M. 360/65 computer by means of a least-squares Algol program for overlapping X-ray powder reflections, written by Rietveld (R.C.N. Petten, the Netherlands). Table V-1 gives, as an example, the observed and calculated values for $10^5 \sin^2\theta$ and for the intensities of Pr_2S_3 and Pr_3S_4. The calculated values are based on a model having the thorium phosphide structure with the space group $I\bar{4}3d$ (T_d^6) comprising the sulphur atoms at the 16c position, with 1/12 as the value for the parameter, and the metal atoms having the position 12a. For the compositions showing metal-site vacancies, the calculated values are based on a model with a statistical

55

h k l	Pr$_2$S$_3$				Pr$_3$S$_4$			
	I$_{calc}$	I$_{obs}$	$10^5\sin^2\Theta$ calc	obs	I$_{calc}$	I$_{obs}$	$10^5\sin^2\Theta$ calc	obs
2 1 1	1000	v.s.	4848	4831	1000	v.s.	4845	4837
2 2 0	140	m.	6464	6454	140	m.	6460	6452
3 1 0	997	v.s.	8080	8073	902	v.s.	8075	8067
3 2 1	504	v.s.	11312	11305	447	v.s.	11305	11292
4 0 0	16	v.w.	12907	12933	17	v.w.	12899	12919
4 2 0	445	v.s.	16133	16139	420	s.	16124	16124
3 3 2	256	s.	17747	17738	240	s.	17734	17734
4 2 2	70	w.	19360	19364	66	w.	19348	19348
4 3 1	183 }	s.	20973	20974	175 }	s.	20961	20944
5 1 0	86 }				86 }			
5 2 1	145	m.	24200	24213	138	m.	24185	24204
4 4 0	16	v.w.	25813	25846	16	v.w.	25798	25837
5 3 0	4	n.o.	27368	n.o.	3	n.o.	27410	n.o.
5 3 2	189 }	s.	30653	30635	177 }	s.	30635	30632
6 1 1	113 }				104 }			
6 2 0	57	w.	32267	32256	51	w.	32247	32245
5 4 1	150	m.	33865	33865	157	m.	33860	33838
6 3 1	62	w.	37107	37104	57	w.	37084	37076
4 4 4	70	w.	38720	38730	66	w.	38702	38702
5 4 3	7 }	n.o.	40247	n.o.	6 }	n.o.	40309	n.o.
7 1 0	2 }				1 }			
6 4 0	77	w.	41947	41948	73	w.	41921	41929
5 5 2	47 }				44 }			
6 3 3	48 }	m.	43560	43546	45 }	m.	43534	43527
7 2 1	96 }				90 }			
6 4 2	53	w.	45174	45167	48	w.	45146	45147
7 3 0	20	v.w.	46787	46803	20	v.w.	46758	46756

Table V-1. Observed and calculated intensities and $10^5\sin^2\Theta$
values of Pr$_2$S$_3$ and Pr$_3$S$_4$.

distribution of the vacancies over the metal sites. The agreement between
the observed and calculated data is fairly good.

V-3-1.   The system CaPr$_2$S$_4$-BaPr$_2$S$_4$-Pr$_{2 2/3}$S$_4$-Pr$_3$S$_4$.

The compositions investigated in this system are indicated in
figure V-2. In order to obtain these compositions we first prepared
as starting materials Pr$_{2 2/3}$S$_4$, Pr$_3$S$_4$, CaPr$_2$S$_4$ and BaPr$_2$S$_4$. Pr$_3$S$_4$ was
prepared by heating a mixture of the elements in an evacuated silica
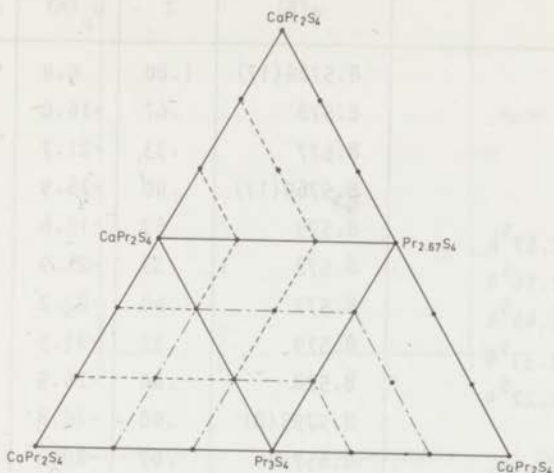
Fig. V-2. *Compositions investigated in the quaternary system*
$CaPr_2S_4$-$BaPr_2S_4$-Pr_3S_4-Pr_2S_3. *Dash-dot lines indicate*
planes of equal electron concentration and dashed lines
indicate planes of equal interatomic distances.

ampoule, according to method 1 (chapter V-1). $Pr_{2/3}S_4$, $CaPr_2S_4$ and
$BaPr_2S_4$ were prepared by reaction of dry hydrogen sulphide and praseo-
dymium oxide or mixtures of praseodymium oxide and calcium carbonate
or barium carbonate according to method 3 (chapter V-1). The intermediate
compositions were prepared by a solid state reaction of compressed mix-
tures of the starting materials (method 6, chapter V-1).

Magnetic susceptibility measurements were carried out by means of
the Faraday-balance in the temperature range of 80 - 1000 K, in which
temperature range all compositions showed a Curie-Weiss behaviour.

The cell edge, paramagnetic Curie-temperature and the effective
magnetic moment per rare earth ion of the investigated compositions are
indicated in table V-2. In this table we have also indicated the
conduction electron concentration as can be calculated from a simple
ionic model with trivalent praseodymium and divalent calcium, strontium
and barium. In this table we have also indicated the corresponding data
for $SrPr_2S_4$.

	a(Å)	Z	Θ_p(K)	$\mu_{eff}(\mu_B)$
Pr_3S_4	8.5786(17)	1.00	0.0	3.56
$Pr_{2.98}S_4$	8.578	.67	-16.0	3.55
$Pr_{2.78}S_4$	8.577	.33	-21.7	3.58
$Pr_{2.67}S_4$	8.5760(17)	.00	-26.9	3.59
$Ca_{0.33}Pr_{2.67}S_4$	8.579	.67	-15.6	3.58
$Ca_{0.33}Pr_{2.56}S_4$	8.578	.33	-21.9	3.59
$Ca_{0.33}Pr_{2.44}S_4$	8.577	.00	-27.2	3.60
$Ca_{0.67}Pr_{2.33}S_4$	8.579	.33	-21.5	3.59
$Ca_{0.67}Pr_{2.22}S_4$	8.578	.00	-26.5	3.60
$CaPr_2S_4$	8.5793(8)	.00	-26.8	3.59
$Ba_{0.33}Pr_{2.67}S_4$	8.657	.67	-20.3	3.57
$Ba_{0.33}Pr_{2.56}S_4$	8.656	.33	-27.4	3.58
$Ba_{0.33}Pr_{2.44}S_4$	8.655	.00	-27.6	3.61
$Ba_{0.33}Ca_{0.33}Pr_{2.22}S_4$	8.657	.00	-27.6	3.60
$Ba_{0.33}Ca_{0.67}Pr_2S_4$	8.657	.00	-27.5	3.60
$Ba_{0.33}Ca_{0.33}Pr_{2.33}S_4$	8.657	.33	-28.2	3.58
$Ba_{0.67}Pr_{2.33}S_4$	8.735	.33	-28.6	3.59
$Ba_{0.67}Pr_{2.22}S_4$	8.734	.00	-26.9	3.59
$Ba_{0.67}Ca_{0.33}Pr_2S_4$	8.736	.00	-27.1	3.59
$BaPr_2S_4$	8.8136(18)	.00	-26.2	3.60
$SrPr_2S_4$	8.6817(15)	.00	-26.5	3.61

Table V-2. Cell edge (a), assumed number of conduction electrons per formula unit (Z), paramagnetic Curie-temperature (Θ_p) and the effective magnetic moment (μ_{eff}) of some compositions in the series Pr_3S_4-Pr_2S_3-$CaPr_2S_4$-$BaPr_2S_4$.

In figure V-3 the paramagnetic Curie-temperature of these compositions is given as a function of the conduction electron concentration for the different series of values for the cell edge.

Low temperature magnetic measurements were performed by means of the P.A.R. vibrating sample magnetometer on samples of Pr_3S_4, $Pr_{2\,2/3}S_4$, $CaPr_2S_4$, $SrPr_2S_4$ and $BaPr_2S_4$. The results of some of these measurements
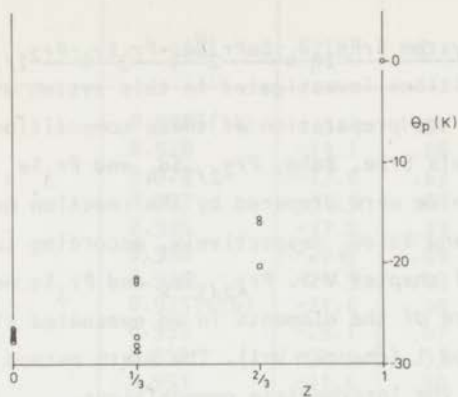
Fig. V-3. *The paramagnetic Curie-temperature (θ_p) versus the assumed number of conduction electrons for compositions investigated in the series $CaPr_2S_4$-$BaPr_2S_4$-Pr_3S_4-Pr_2S_3. ○: compositions with a = 8.578 Å, ◌: compositions with a = 8.657 Å, △: compositions with a = 8.735 Å.*
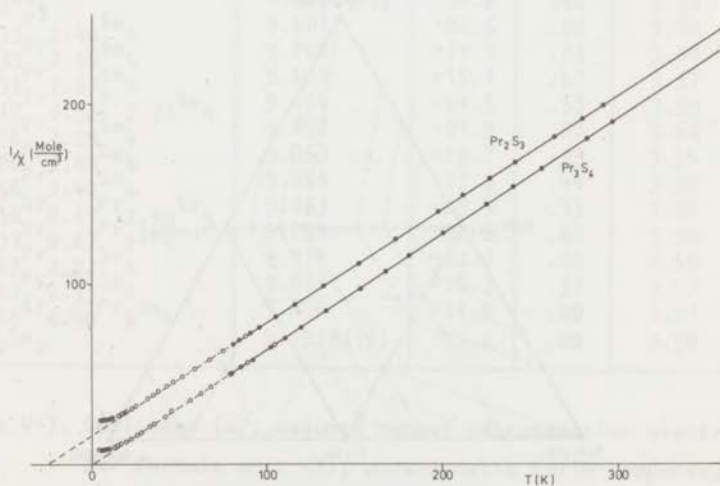
Fig. V-4. *The $1/\chi$ versus T curves for Pr_2S_3 and Pr_3S_4. •: obtained from measurements with the Faraday balance; ○: obtained from measurements with the vibrating sample magnetometer.*

are summarized in figure V-4.

V-3-2. The system $SrPr_2Se_4-BaPr_2Se_4-Pr_3Se_4-Pr_{2\,2/3}Se_4$.

The compositions investigated in this system are indicated in
figure V-5. For the preparation of these compositions we used as
starting materials SrSe, BaSe, $Pr_{2\,2/3}Se_4$ and Pr_3Se_4. Strontium selenide
and barium selenide were prepared by the reaction between dry hydrogen
gas and $SrSeO_4$ and $BaSeO_4$ respectively, according to the fifth prepa-
ration method of chapter V-1. $Pr_{2\,2/3}Se_4$ and Pr_3Se were prepared by
heating a mixture of the elements in an evacuated silica ampoule, ac-
cording to method 1 (chapter V-1). The sixth method of chapter V-1 was
used to prepare the intermediate compositions.

The results of magnetic susceptibility measurements, carried out
by means of the Faraday balance in the temperature range of 80 - 1000 K,
are given in figure V-6 and table V-4. In that temperature range a
Curie-Weiss law is obeyed. In table V-3 is also indicated the cell
edge and the conduction electron concentration based on a simple ionic
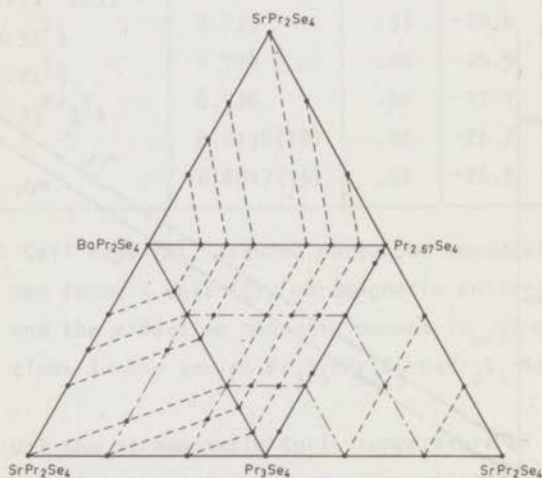
Fig. V-5. *Compositions investigated in the quaternary system*
$SrPr_2Se_4-BaPr_2Se_4-Pr_3Se_4-Pr_2Se_3$. Dash-dot lines indicate
planes of equal electron concentration and dashed lines
indicated planes of equal interatomic distances.

	a(Å)	Θ_p(K)	Z	μ_{eff}(μ_B)
Pr_3Se_4	8.9288(14)	- 3.1	1.00	3.52
$Pr_{2.96}Se_4$	8.928	-13.1	.88	3.54
$Pr_{2.89}Se_4$	8.928	-27.0	.67	3.56
$Pr_{2.87}Se_4$	8.927	-31.5	.61	3.56
$Pr_{2.78}Se_4$	8.926	-37.2	.33	3.58
$Pr_{2.70}Se_4$	8.926	-26.7	.09	3.55
$Pr_{2.68}Se_4$	8.925	-24.3	.03	3.59
$Pr_{2.67}Se_4$	8.9251(16)	-21.6	.00	3.58
$Sr_{0.33}Pr_{2.67}Se_4$	8.953	-25.1	.67	3.57
$Sr_{0.33}Pr_{2.56}Se_4$	8.952	-32.1	.33	3.58
$Sr_{0.33}Pr_{2.44}Se_4$	8.951	-21.6	.00	3.58
$Ba_{0.12}Pr_{2.59}Se_4$	8.952	-22.3	.00	3.59
$Ba_{0.12}Pr_{2.70}Se_4$	8.954	-31.5	.33	3.58
$Ba_{0.12}Pr_{2.81}Se_4$	8.955	-25.0	.67	3.57
$Ba_{0.12}Pr_{2.88}Se_4$	8.956	-11.7	.88	3.55
$Sr_{0.67}Pr_{2.33}Se_4$	8.978	-26.7	.33	3.58
$Sr_{0.67}Pr_{2.22}Se_4$	8.977	-22.0	.00	3.60
$Ba_{0.22}Pr_{2.52}Se_4$	8.975	-21.7	.00	3.59
$Ba_{0.22}Pr_{2.63}Se_4$	8.976	-26.3	.33	3.57
$Ba_{0.22}Pr_{2.74}Se_4$	8.977	-19.1	.67	3.56
$Ba_{0.22}Pr_{2.78}Se_4$	8.978	-16.3	.78	3.56
$Ba_{0.17}Sr_{0.16}Pr_{2.67}Se_4$	8.977	-20.1	.67	3.56
$SrPr_2Se_4$	9.0027(17)	-21.6	.00	3.58
$Ba_{0.33}Pr_{2.44}Se_4$	9.001	-22.5	.00	3.60
$Ba_{0.33}Pr_{2.56}Se_4$	9.002	-21.3	.33	3.58
$Ba_{0.33}Pr_{2.67}Se_4$	9.003	-15.1	.67	3.57
$Ba_{0.17}Sr_{0.50}Pr_{2.33}Se_4$	9.004	-21.5	.33	3.59
$Ba_{0.56}Pr_{2.29}Se_4$	9.052	-21.9	.00	3.60
$Ba_{0.56}Pr_{2.40}Se_4$	9.053	-19.7	.33	3.59
$Ba_{0.56}Pr_{2.44}Se_4$	9.054	-17.6	.44	3.59
$Ba_{0.50}Sr_{0.17}Pr_{2.33}Se_4$	9.053	-19.9	.33	3.58
$Ba_{0.33}Sr_{0.67}Pr_2Se_4$	9.052	-22.6	.00	3.59
$Ba_{0.67}Pr_{2.22}Se_4$	9.076	-22.0	.00	3.59
$Ba_{0.67}Pr_{2.33}Se_4$	9.078	-18.7	.33	3.57
$Ba_{0.50}Sr_{0.50}Pr_2Se_4$	9.078	-21.0	.00	3.57
$BaPr_2Se_4$	9.1518(15)	-22.2	.00	3.58

Table V-3. Cell edge (a), assumed number of conduction electrons
per formula unit (Z), paramagnetic Curie-temperature
(Θ_p) and the effective magnetic moment in the series
Pr_3Se_4-Pr_2Se_3-$SrPr_2Se_4$-$BaPr_2Se_4$
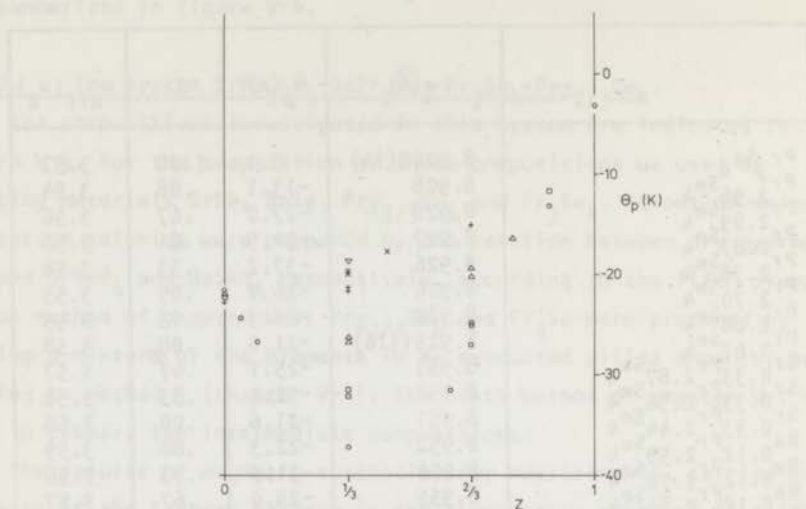
Fig. V-6. *The paramagnetic Curie-temperature (θ_p) versus the assumed number of conduction electrons for compositions investigated in the series $SrPr_2Se_4$-$BaPr_2Se_4$-Pr_3Se_4-Pr_2Se_3. ∘ : compositions with $a = 8.927$ Å; ○ : compositions with $a = 8.953$ Å, Δ : compositions with $a = 8.977$ Å; + : compositions with $a = 9.003$ Å; × : compositions with $a = 9.053$ Å; ∇ : compositions with $a = 9.078$ Å.*

model comprising trivalent praseodymium.

In this system low temperature magnetic measurements were performed on samples of Pr_3Se_4, $Pr_{22/3}Se_4$, $SrPr_2Se_4$ and $BaPr_2Se_4$ by means of the P.A.R. magnetometer. The results of these measurements are summarized in figures V-7 and V-8.

For Pr_3Se_4 Loginov and Sergeeva (3) have reported +6 K and 3.43 μ_B as values for the paramagnetic Curie-temperature and the effective magnetic moment respectively.

V-3-3.   The system $CaNd_2S_4$-$BaNd_2S_4$-Nd_3S_4-$Nd_{22/3}S_4$.

The compositions investigated in this system are given in figure V-9. These compositions were prepared in an analogous way as those in the system $CaPr_2S_4$-$BaPr_2S_4$-Pr_3S_4-$Pr_{22/3}S_4$ (chapter V-3-1).

Magnetic susceptibility measurements were carried out by means of

62
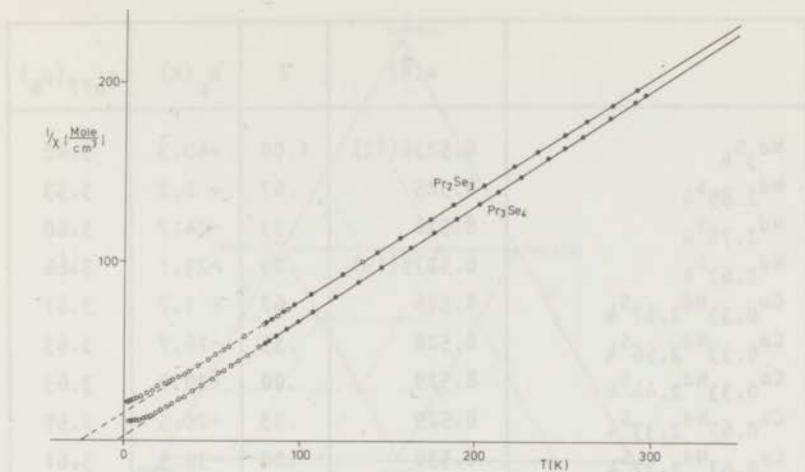
Fig. V-7. *The $1/\chi$ versus T curves for Pr_2Se_3 and Pr_3Se_4.*
   • : obtained from measurements with the Faraday balance;
   ∘ : obtained from measurements with the vibrating
   sample magnetometer.
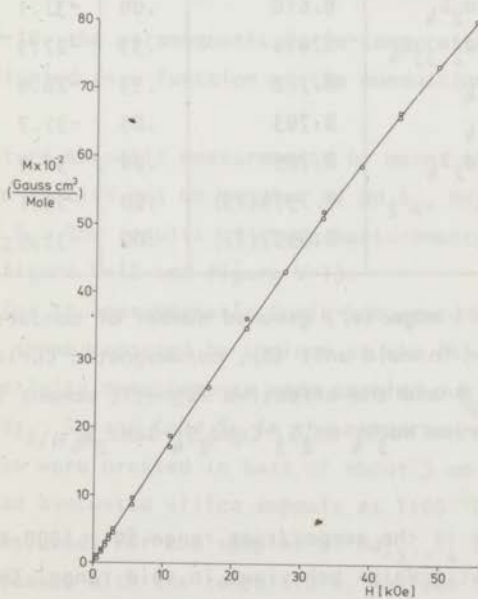
Fig. V-8. *The magnetization (M) versus the magnetic field (H)*
   for Pr_2Se_3. T = 1.95 K.

	$a(\text{Å})$	Z	$\Theta_p(K)$	$\mu_{eff}(\mu_B)$
Nd_3S_4	8.5236(12)	1.00	+40.3	3.42
$Nd_{2.89}S_4$	8.525	.67	+ 2.2	3.53
$Nd_{2.78}S_4$	8.526	.33	-24.7	3.60
$Nd_{2.67}S_4$	8.5275(19)	.00	-29.1	3.66
$Ca_{0.33}Nd_{2.67}S_4$	8.526	.67	+ 1.7	3.61
$Ca_{0.33}Nd_{2.56}S_4$	8.528	.33	-26.7	3.63
$Ca_{0.33}Nd_{2.44}S_4$	8.529	.00	-29.7	3.63
$Ca_{0.67}Nd_{2.33}S_4$	8.529	.33	-26.5	3.59
$Ca_{0.67}Nd_{2.22}S_4$	8.530	.00	-30.5	3.61
$CaNd_2S_4$	8.5315(13)	.00	-30.7	3.63
$Ba_{0.33}Nd_{2.67}S_4$	8.613	.67	+ 0.9	3.55
$Ba_{0.33}Nd_{2.56}S_4$	8.614	.33	-27.7	3.61
$Ba_{0.33}Nd_{2.44}S_4$	8.616	.00	-31.1	3.60
$Ba_{0.33}Ca_{0.33}Nd_{2.22}S_4$	8.617	.00	-30.8	3.60
$Ba_{0.33}Ca_{0.67}Nd_2S_4$	8.618	.00	-31.1	3.59
$Ba_{0.33}Ca_{0.33}Nd_{2.33}S_4$	8.616	.33	-27.3	3.58
$Ba_{0.67}Nd_{2.33}S_4$	8.702	.33	-28.0	3.58
$Ba_{0.67}Nd_{2.22}S_4$	8.703	.00	-31.7	3.60
$Ba_{0.67}Ca_{0.33}Nd_2S_4$	8.705	.00	-31.9	3.61
$BaNd_2S_4$	8.7914(13)	.00	-32.1	3.60
$SrNd_2S_4$	8.6537(11)	.00	-31.5	3.62

Table V-4. Cell edge (a), assumed number of conduction electrons
per formula unit (Z), paramagnetic Curie-temperature
(Θ_p) and the effective magnetic moment (μ_{eff}) in the
series Nd_3S_4-Nd_2S_3-$CaNd_2S_4$-$BaNd_2S_4$.

the Faraday balance in the temperature range 80 - 1000 K. All compo-
sitions showed a Curie-Weiss behaviour in said range. The cell edge,
paramagnetic Curie-temperature, the effective magnetic moment per ion and
the number of conduction electrons per formula unit are given in table
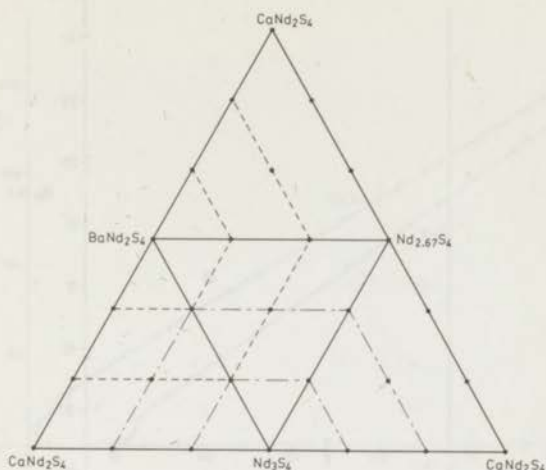
Fig. V-9. *Compositions investigated in the quaternary system*
$CaNd_2S_4$-$BaNd_2S_4$-Nd_3S_4-Nd_2S_3. *Dash-dot lines indicate*
planes of equal electron concentration and dashed lines
indicate planes of equal interatomic distances.

V-4. In figure V-10, the paramagnetic Curie-temperature of these com-
positions is indicated as a function of the conduction electron con-
centration.

Low temperature magnetic measurements by means of the P.A.R.
magnetometer were carried out on samples of Nd_3S_4, $Nd_{2\,2/3}S_4$, $CaNd_2S_4$,
$SrNd_2S_4$ and $BaNd_2S_4$. The results of these measurements are summarized
in figure V-11, figure V-12 and figure V-13.

Our values for the paramagnetic Curie-temperature for Nd_3S_4 and
Nd_2S_3 agree with those reported by Loginov et al. (4).

Rough conductivity measurements were carried out on powdered sam-
ples of Nd_3S_4, $Nd_{2\,2/3}S_4$ and $CaNd_2S_4$ in the temperature range of 80 -
300 K. The samples were pressed in bars of about 3 mm x 3 mm x 15 mm
and sintered in an evacuated silica ampoule at 1100 $^{\circ}$C. The four-point-
contact method was used. For the samples of $Nd_{2\,2/3}S_4$ and $CaNd_2S_4$ the
conductivity decreased with the temperature, whereas for Nd_3S_4 the
conductivity increased with decreasing temperature. For $Nd_{2\,2/3}S_4$ and
$CaNd_2S_4$ the resistivity was in the order of $1 - 10^{-1}$ Ωcm and for Nd_3S_4
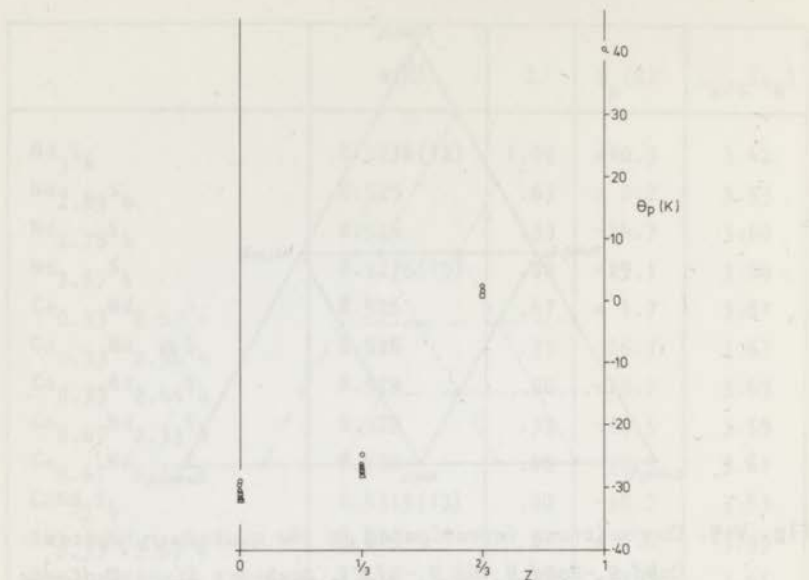
Fig. V-10. *The paramagnetic Curie-temperature (Θ_p) versus the assumed number of conduction electrons for compositions investigated in the series $CaNd_2S_4$-$BaNd_2S_4$-Nd_3S_4-Nd_2S_3. ∘ : compositions with $a = 8.526$ Å; ∘ : compositions with $a = 8.616$ Å; Δ : compositions with $a = 8.703$ Å.*

we found $10^{-2} - 10^{-3}$ Ωcm. No discontinuity in the resistivity as a function of the temperature was observed. The values of the resistivity give only a rough information and depend strongly on the preparation method of the bars. Picon and Flahaut have found 1.2×10^{-6} Ωcm for the resistivity of Nd_3S_4 (5).

V-3-4.   The system $SrNd_2Se_4$-$BaNd_2Se_4$-Nd_3Se_4-$Nd_{2/3}Se_4$.

The compositions investigated in this system are given in figure V-14. These compositions were prepared in an analogous manner as those in the system $SrPr_2Se_4$-$BaPr_2Se_4$-Pr_3Se_4-$Pr_{2/3}Se_4$ (chapter V-3-2).

Magnetic susceptibility measurements were carried out by means of the Faraday balance in the temperature range of 80 - 1000 K. All compositions showed a Curie-Weiss behaviour in that region. The cell
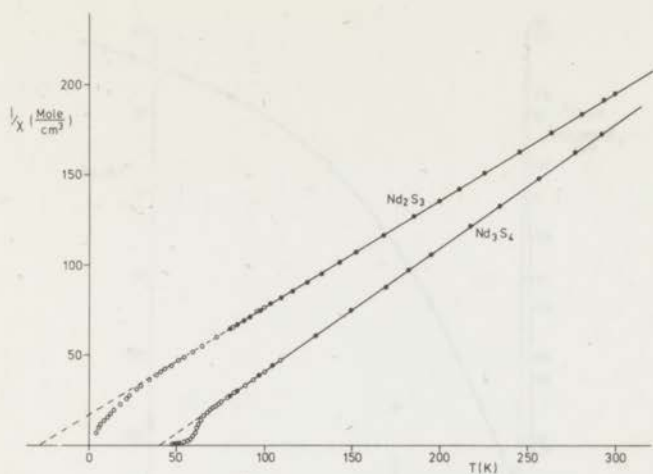
Fig. V-11. *The $1/\chi$ versus T curves for Nd_2S_3 and Nd_3S_4.* •:*obtained from measurements with the Faraday balance;* ○:*obtained from measurements with the vibrating sample magnetometer.*
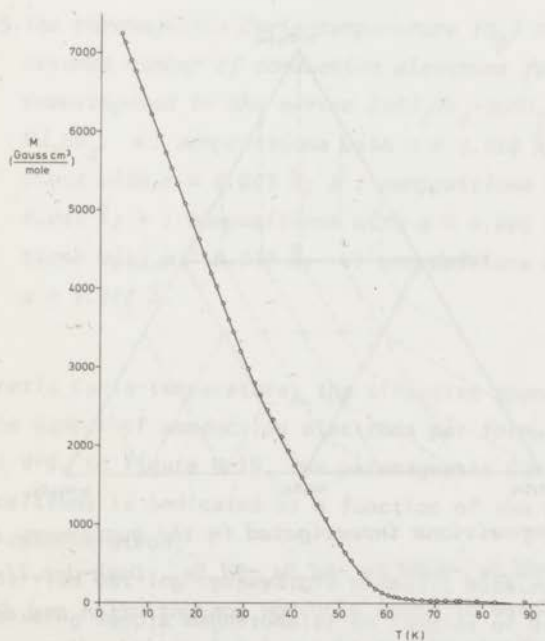
Fig. V-12. *The magnetization (M) versus the temperature (T) for Nd_3S_4.*
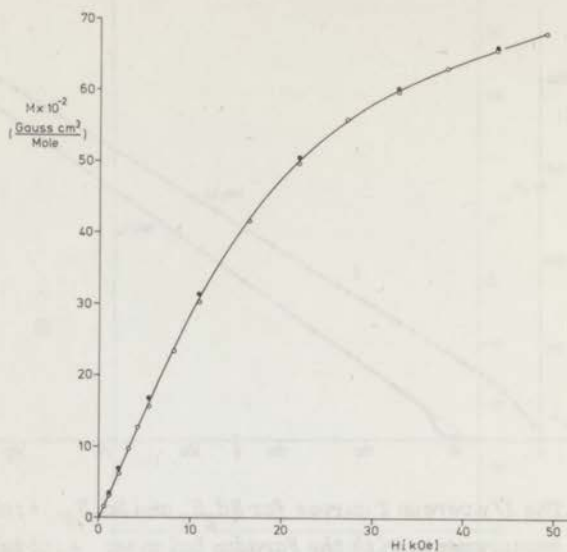
Fig. V-13. *The magnetization per Nd (M) versus the magnetic field*
(H) for BaNd$_2$S$_4$. T = 2.05 K.
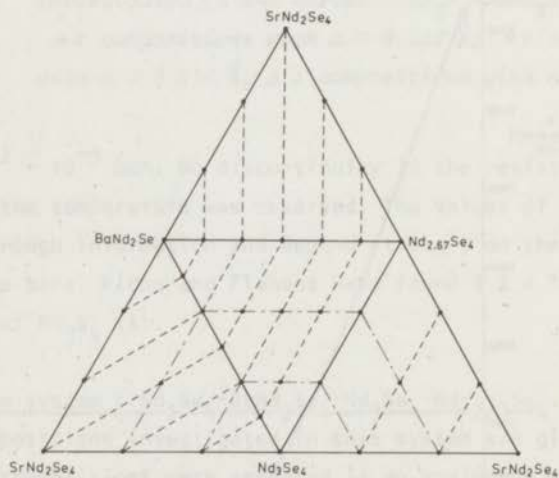
Fig. V-14. *Compositions investigated in the quaternary system*
SrNd$_2$Se$_4$-BaNd$_2$Se$_4$-Nd$_3$Se$_4$-Nd$_2$Se$_3$. Dash-dot lines indicate
planes of equal electron concentration and dashed lines
indicate planes of equal interatomic distances.

68
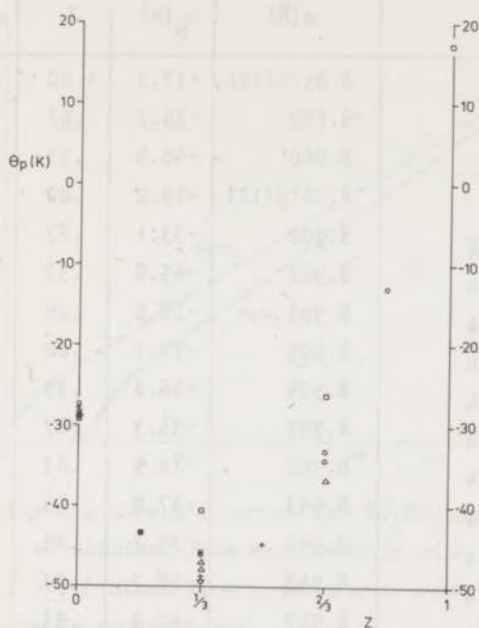
Fig. V-15. *The paramagnetic Curie-temperature (θ_p) versus the assumed number of conduction electrons for compositions investigated in the series $SrNd_2Se_4$-$BaNd_2Se_4$-Nd_3Se_4-Nd_2Se_3. ○: compositions with $a = 8.859$ Å; ○: compositions with $a = 8.902$ Å; Δ : compositions with $a = 8.945$ Å; + : compositions with $a = 8.990$ Å; ▽ : compositions with $a = 9.033$ Å; •: compositions with $a = 9.076$ Å.*

edge, paramagnetic Curie-temperature, the effective magnetic moment per ion and the number of conduction electrons per formula unit are given in table V-5. In figure V-15, the paramagnetic Curie-temperature of these compositions is indicated as a function of the assumed conduction electron concentration.

We have carried out low temperature magnetic measurements using the P.A.R. vibrating sample magnetometer on samples of Nd_3Se_4, $Nd_{22/3}Se_4$, $SrNd_2Se_4$ and $BaNd_2Se_4$. The results of these measurements are given in figure V-16, figure V-17 and figure V-18.

69

	$a(\text{Å})$	$\theta_p(K)$	Z	$\mu_{eff}(\mu_B)$
Nd_3Se_4	8.8576(19)	+17.2	1.00	3.40
$Nd_{2.89}Se_4$	8.859	-26.2	.67	3.56
$Nd_{2.78}Se_4$	8.860	-40.6	.33	3.63
$Nd_{2.67}Se_4$	8.8619(12)	-29.2	.00	3.62
$Sr_{0.33}Nd_{2.67}Se_4$	8.900	-33.1	.67	3.57
$Sr_{0.33}Nd_{2.56}Se_4$	8.902	-45.8	.33	3.59
$Sr_{0.33}Nd_{2.44}Se_4$	8.903	-28.6	.00	3.60
$Ba_{0.17}Nd_{2.56}Se_4$	8.905	-27.1	.00	3.61
$Ba_{0.17}Nd_{2.67}Se_4$	8.904	-46.0	.33	3.58
$Ba_{0.17}Nd_{2.78}Se_4$	8.902	-34.3	.67	3.57
$Ba_{0.17}Nd_{2.83}Se_4$	8.902	-12.9	.83	3.54
$Sr_{0.67}Nd_{2.33}Se_4$	8.943	-47.0	.33	3.61
$Sr_{0.67}Nd_{2.22}Se_4$	8.944	-29.2	.00	3.61
$Ba_{0.33}Nd_{2.44}Se_4$	8.948	-28.7	.00	3.60
$Ba_{0.33}Nd_{2.56}Se_4$	8.947	-47.9	.33	3.59
$Ba_{0.33}Nd_{2.67}Se_4$	8.945	-36.7	.67	3.56
$SrNd_2Se_4$	8.9857(16)	-27.2	.00	3.62
$Ba_{0.50}Nd_{2.33}Se_4$	8.991	-27.9	.00	3.61
$Ba_{0.50}Nd_{2.44}Se_4$	8.990	-49.1	.33	3.59
$Ba_{0.50}Nd_{2.50}Se_4$	8.989	-43.8	.50	3.58
$Ba_{0.33}Sr_{0.33}Nd_{2.33}Se_4$	8.988	-26.7	.33	3.60
$Ba_{0.33}Sr_{0.67}Nd_2Se_4$	9.031	-27.8	.00	3.61
$Ba_{0.67}N_{2.22}Se_4$	9.035	-29.0	.00	3.60
$Ba_{0.67}Nd_{2.33}Se_4$	9.033	-49.5	.33	3.58
$Ba_{0.67}Sr_{0.33}Nd_2Se_4$	9.076	-28.4	.00	3.62
$Ba_{0.83}Nd_{2.11}Se_4$	9.078	-28.1	.00	3.61
$Ba_{0.83}Nd_{2.17}Se_4$	9.076	-42.7	.17	3.60
$BaNd_2Se_4$	9.1211(11)	-29.2	.00	3.62

Table V-5. Cell edge (a), assumed number of conduction electrons
per formula unit (Z), paramagnetic Curie-temperature
(θ_p) and the effective magnetic moment (μ_{eff}) in the
series Nd_3Se_4-Nd_2Se_3-$SrNd_2Se_4$-$BaNd_2Se_4$.

In this sector the only possible values for x are in the range
0.23 < x < 0.27. Figure V-16 shows the results of the susceptibility
measurements. For the extreme compositions in this sector in the
temperature interval of 80 - 360°K the values observed were 100 <
p_c < 105, θ_p = -0.29 for Nd₂Se₃ and 102 < p_c < 105, θ_p = 0.11
for Nd₃Se₄.

References

1. ...
2. ...
3. ...
4. ...
5. ...
6. ...
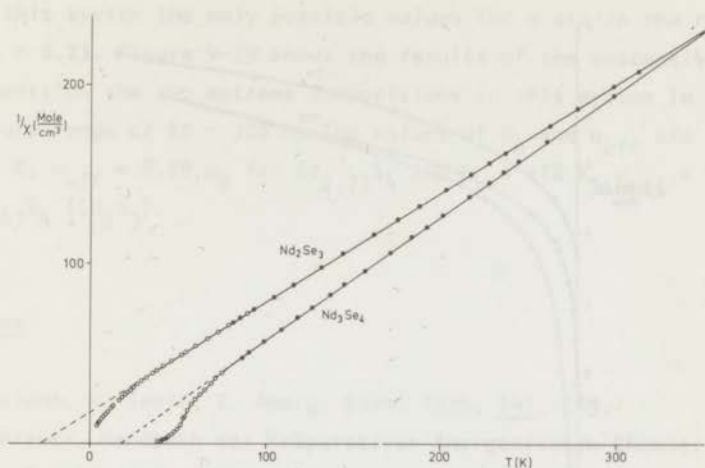
Fig. V-16. *The 1/χ versus T curves for Nd₂Se₃ and Nd₃Se₄.*
•: obtained from measurements with the Faraday balance;
∘: obtained from measurements with the vibrating
sample magnetometer.
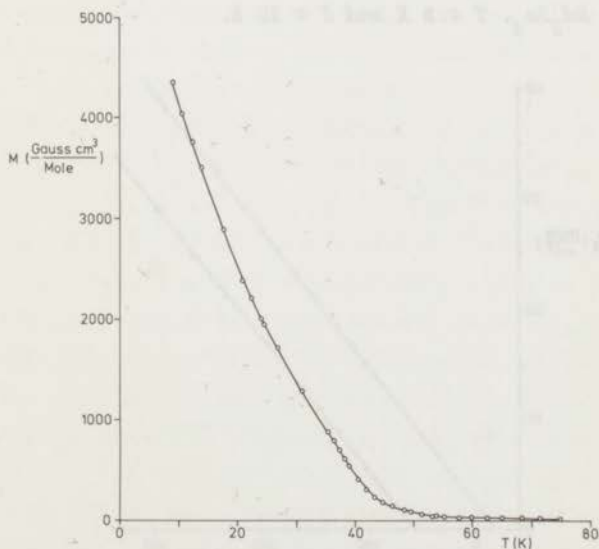
Fig. V-17. *The magnetization (M) versus the temperature (T) for*
Nd₃Se₄.

71
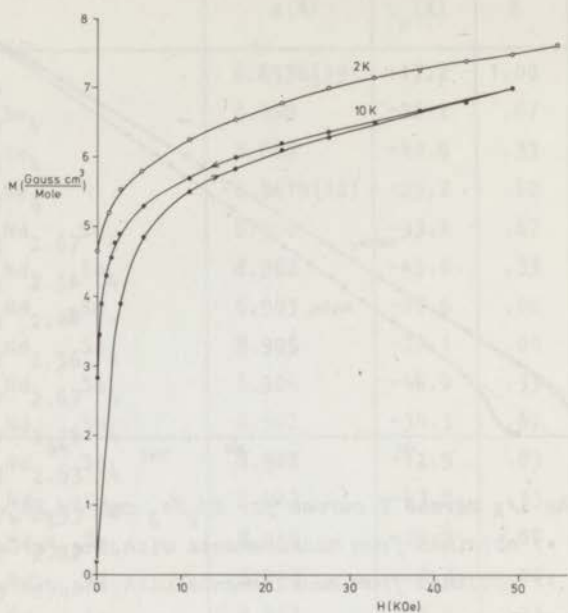
Fig. V-18.*The magnetization (M) versus the magnetic field (H) for Nd_3Se_4. T = 2 K and T = 10 K.*
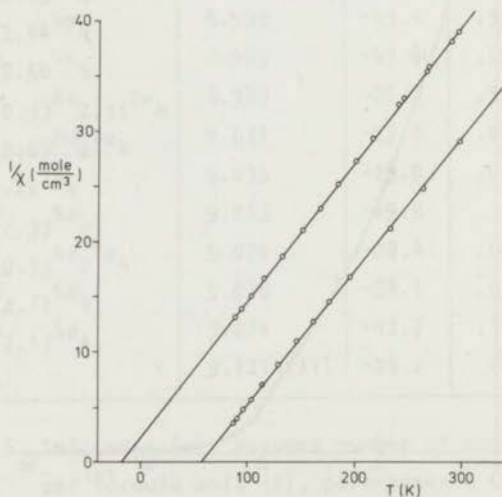
Fig. V-19.*The $1/\chi$ versus T curves for Gd_2S_3 (upper) and for $Gd_{2.77}S_4$ (lower).*

<u>V-3-5.</u>   The system $Gd_{3-x}S_4$.

In this system the only possible values for x are in the range
$0.33 > x > 0.23$. Figure V-19 shows the results of the susceptibility
measurements on the two extreme compositions in this system in the
temperature range of 80 - 300 K. The values of Θ_p and μ_{eff} are
$\Theta_p = +57$ K, $\mu_{eff} = 8.28$ μ_B for $Gd_{2.77}S_4$ and $\Theta_p = -18$ K, $\mu_{eff} = 8.03$ μ_B
for $Gd_{2.67}S_4$ (Gd_2S_3).

<u>References</u>

1. W. Klemm, H. Senff, Z. Anorg. Chem. 1939, <u>241</u>, 259.
2. G. Brauer, Handbuch der Präparativen Anorganischen Chemie.
    Ferdinand Enke Verlag Stuttgart (1960) p. 830.
3. G.M. Loginov, V.M. Sergeeva, Sov. Phys. - Solid State 1971, <u>12</u>, 2191.
4. G.M. Loginov, V.M. Sergeeva, M.F. Bryzhina, Sov. Phys. - Solid
    State 1971, <u>12</u>, 2942.
5. M.C. Picon, J. Flahaut, Compt. Rend. 1956, <u>243</u>, 2074.

DISCUSSION

VI-1. Introduction.

From the magnetic data obtained for the rare earth chalcogenides it is clear that a certain relationship exists between the ratio of rare earth ions to chalcogen ions and the paramagnetic Curie-temperature. As the number of electrons in the conduction band is also related to this ratio it is obvious to check if there is a relation between the number of conduction electrons and the paramagnetic Curie-temperature. The influence of the magnitude of the cell edge, being a function of size and ratio of cations and anions, must be considered as well. A theoretical relation between the conduction electron concentration and the paramagnetic Curie-temperature for a metallic compound is given by the RKKY-theory as is indicated in chapter II (eq. II-28).

The summation of eq. II-28 over all metal positions in the thorium-phosphide structure has been carried out for various values of the Fermi-vector (k_F) and the cell edge of the cubic unit cell. Due to the convergency the summations could be limited to a sphere with a radius of 25 $\overset{o}{A}$. The results are graphically represented in figure VI-1. As the theoretical value for k_F, based on a model with free conduction electrons is zero for L_2X_3 and approximately 0.6 $\overset{o}{A}^{-1}$ for L_3X_4, we expected an increasing positive interaction between the lanthanide ions when the conduction band is filled and consequently we expected an increasing value for the paramagnetic Curie-temperature on going from L_2X_3 to L_3X_4. As can be seen from figure V-10 and figure V-19 the values for the paramagnetic Curie-temperature rise when we go from Nd_2S_3 to Nd_3S_4 and when we go from Gd_2S_3 to $Gd_{2.77}S_4$. Going from Pr_2S_3 to Pr_3S_4 a similar behaviour is shown, although a slight minimum can be observed for $Z = 1/3$ in some

RKKY-sum

0.5

0

-0.5

-1.0

-1.5

-2.0

-2.5

-3.0

0.3 0.4 0.5 0.6 0.7 0.8 0.9 1.0

k_F
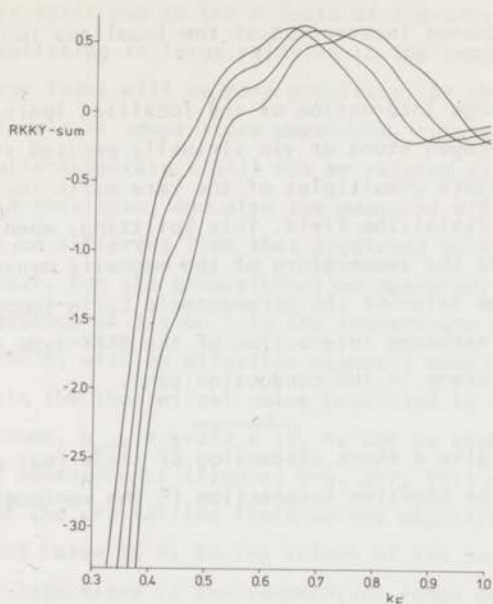
Fig. VI-1. *RKKY-sum versus k_F for the metal positions in the thorium-
phosphide structure for different values of the cubic
cell edge.*

of the series in that system (figure V-3). However, the curves of the
paramagnetic Curie-temperature versus the number of conduction electrons
for the selenide series Pr_2Se_3-Pr_3Se_4 and Nd_2Se_3-Nd_3Se_4 show a deviation
from this behaviour (figures V-6 and V-15). Here we see a small negative
value of the paramagnetic Curie-temperature for the compounds Pr_2Se_3
and Nd_2Se_3. These values are of the same order of magnitude as the
values found for the compositions L_2S_3. However, when in the selenide
compositions the metal content is increased, the paramagnetic Curie-
temperature first becomes more negative. This is not the expected beha-
viour on applying the RKKY-theory on these compositions. Thus a new
theoretical interpretation must be found.

First we have to find an explanation for the negative values of
the paramagnetic Curie-temperature which we have found for the semi-
conducting compounds L_2X_3 and ML_2X_4. The negative magnetic interactions
in these compounds may be caused by several mechanisms or combinations

75

thereof:

1. A direct exchange interaction of the localized ionic magnetic moments.

2. A superexchange interaction of the localized ionic magnetic moments via the chalcogen atoms or via virtually excited states.

3. The ground state J-multiplet of the rare earth ions can be split due to the crystalline field. This splitting, when large in comparison to the temperature of the magnetic measurements, will influence the value of the paramagnetic Curie-temperature.

4. An indirect exchange interaction of the RKKY-type due to thermally excited electrons in the conduction band.

We will now give a short discussion of these four possibilities which may cause the negative interaction in the semiconducting compositions:

ad 1.   A direct exchange interaction between the rare earth ions can be neglected for two reasons.

a.   The distance between the rare earth ions in these compounds is large. Rare earth compounds having comparable distances between the rare earth ions generally show smaller values for the paramagnetic Curie-temperature. For example $NdCl_3$ shows a paramagnetic behaviour to 2.5 K with a paramagnetic Curie-temperature of 0.00 K ± 0.01. The Nd-Nd nearest neighbour distance is 4.231 Å. For $PrCl_3$ having approximately the same nearest neighbour distance the value for θ_p is 0.50 K ± 0.01 (1).

b.   Direct exchange interaction in the rare earth compounds (the cerium compounds excluded) is small due to the deep-lying 4f-electrons which are well-screened by the outer 5p- and 5s-electrons.

ad 2.   Super exchange optionally combined with an indirect exchange mechanism of the RKKY-type is possible for the semiconducting compounds. A theory for this type of interaction has been worked out by Gonçalves da Silva and Falicov (2). A brief summary of this theory will be given in section VI-2.

ad 3.   The degenerate energy levels of the J-multiplet of the ground

state can be split due to the effects of the crystalline field.
When this splitting is large relative to the temperature, the
lowest energy level will be more populated. As the population of
the split levels is temperature dependent, the value of the para-
magnetic Curie-temperature will not be related to the exchange in-
teraction in that case, and also the measured effective magnetic
moment will be different from that predicted by the Russel-Saunders
coupling model. For the compositions we measured, we have found a
linear dependency of $1/\chi$ on T in the temperature range between
80 K and 1100 K, with an effective magnetic moment that approxi-
mately equals the theoretical value predicted by the Russel-Saunders
coupling scheme, $\mu_{eff} = g\sqrt{J(J + 1)}$. As can be seen from the low
temperature measurements (figures V-4, V-7, V-11 and V-16) the
influence of the crystalline field on the magnetic properties can
only be found below 15 K. So the values of the paramagnetic Curie-
temperature determined in the temperature range between 30 K
and 1100 K are not or only slightly influenced by the effects of
the crystalline field.

ad 4.   The excitation of electrons from the valence band into the
conduction band of a semi-conductor is strongly temperature depen-
dent. Consequently the RKKY-type exchange interaction via thermal-
ly excited electrons will be temperature dependent and consequently
there will not be a linear dependency of $1/\chi$ on T. For the com-
positions under our investigation however we find a linear rela-
tion between $1/\chi$ and T, so a RKKY-type interaction via thermally
excited conduction electrons is not important here.

VI-2. The Gonçalves da Silva and Falicov model.

In this model a system of itinerant electronic states weakly
hybridized with a set of localized electronic states is discussed. The
hamiltonian used by Gonçalves da Silva and Falicov (2) consists of six
different terms:

$$\mathcal{H} = E_g + \mathcal{H}_b + \mathcal{H}_+ + \mathcal{H}_- + \mathcal{H}_c + \mathcal{H}_{hyb}$$

where: E_g represents a constant corresponding to the ground state

energy, $\mathcal{H}_b$ describes the contribution of excited electron- and hole-
states in the conduction band, $\mathcal{H}_+$ and $\mathcal{H}_-$ represent the contribution of
extra electrons respectively extra holes in the ionic levels, $\mathcal{H}_c$ is a
correlation term which makes it impossible that two extra holes or two
extra electrons are present at the same ion and $\mathcal{H}_{hyb}$ provides a hybri-
dization between conductionband-holes and -electrons and localized
ionic states. Fourth order perturbation theory yields a coupling between
the localized magnetic moments that can be described by an exchange
integral. Gonçalves da Silva and Falicov calculated the exchange inte-
gral for the following three simple models.

1.   Free-electron-like conduction band.
      First the authors restricted themselves to a large number of con-
      duction electrons, that is, to a metal. This case gives rise to an
      oscillating indirect interaction between the localized spins of
      the RKKY-type. In the case of a single empty free-electron-like
      conduction band however, that is an insulator or an intrinsic semi-
      conductor, an antiferromagnetic exchange equivalent to Anderson's
      super exchange (3) is obtained. In the intermediate cases both
      effects compete and the resulting magnetic ordering depends on the
      number of conduction electrons.

2.   Free-electron-free-hole-like conduction bands.
      For this model two conduction bands with equal effective masses are
      considered. This model is the exact equivalent for the rare earth
      metals to the Fedders and Martin model (4) for antiferromagnetism
      in systems with itinerant electrons.

3.   s-Like- body-centered tight binding band in a b.c.c. lattice.
      With this model the exchange integral is calculated as a function
      of the Fermi-energy and the hole-energy. For the different values
      of the exchange integral the most stable magnetic ordering is
      predicted by minimization of the classical Heisenberg-energy. A
      summary of the results as obtained by Gonçalves da Silva and Falicov
      is given in table VI-1, as a function of:

$$e_F = \frac{\varepsilon_F}{W} \qquad \text{and} \qquad e_h = \frac{E_h}{W}$$

where: ε_F is the Fermi-energy.

78

e_F \ e_h	0.10	0.30	0.50	0.70	0.90
0.90	− 564 − 318 F − 95	− 84 − 51 F − 19	− 33 − 20 F − 8	− 17 − 11 F − 4	− 11 − 7 F − 3
0.70	− 416 − 53 H 126	− 117 − 32 F 18	− 55 − 17 F 6	− 32 − 11 F 3	− 21 − 7 F 2
0.60	− 236 391 AF3 287	− 102 40 H 53	− 53 11 H 21	− 33 4 H 11	− 22 2 H 7
0.20	1821 665 AF1 − 402	337 220 AF1 − 82	137 110 AF2 − 33	73 66 AF2 − 18	45 44 AF2 − 11
0.00	1645 −7998 AF1 − 50	435 −1692 AF1 − 14	20 −694 AF1 − 8	119 −373 AF1 − 6	76 −231 AF1 − 4
−0.30	−1860 687 H 648	− 306 324 H 75	−109 152 AF2 25	− 51 85 AF2 11	− 27 53 AF2 6
−0.50	− 905 −1029 F 194	− 264 − 100 F 59	−120 − 21 F 27	− 67 − 5 F 15	− 42 0 F 10
−0.70	266 − 448 AF1 − 264	− 70 − 117 F − 29	− 51 − 48 F − 8	− 34 − 25 F − 3	− 24 − 15 F − 1
−0.90	858 335 AF1 27	95 9 AF1 − 15	24 − 36 AF1 − 7	8 − 39 AF1 − 4	2 − 3 AF1 − 3
−1.00	517 248 AF2 92	93 31 AF1 7	32 8 AF1 1	14 3 AF1 0	7 1 AF1 0

Table VI-1. Values for the three nearest neighbour exchange integrals as a function of e_h and e_F in units of $\frac{8N^2}{6}(\frac{V}{W})^3 V$, and the ground state magnetic configuration. AF1, AF2 and AF3 represent three types of antiferromagnetic order, F represents ferromagnetic order and H represents helical order (after Gonçalves da Silva and Falicov (2)).

E_h is the energy difference between a system comprising the ion in the $(4f)^{n-1}$ configuration plus one electron with the energy ε_F and the ionic ground state level.

W is half the band width.

For the calculations, Gonçalves da Silva and Falicov have made the assumptions that there is no orbital degeneracy ($J = \frac{1}{2}$) and that $E_e \gg E_h$. The value $e_F = -1.0$ corresponds to an intrinsic semiconductor. For that value of e_F Gonçalves da Silva and Falicov have found two types of antiferromagnetic ordering depending on the values of e_h. For $e_h \approx 0.1$ and $e_F = -1.0$, the localized level being close to the bottom of the conducting band Gonçalves da Silva and Falicov have predicted for a body centered cubic lattice the antiferromagnetic ordering of figure VI-2a due to a considerable influence of second nearest neighbour interaction. This influence becomes less when the number of conducting electrons increases and the antiferromagnetic ordering of figure VI-2b is obtained. For larger values of e_F ferromagnetism and helical magnetic order are
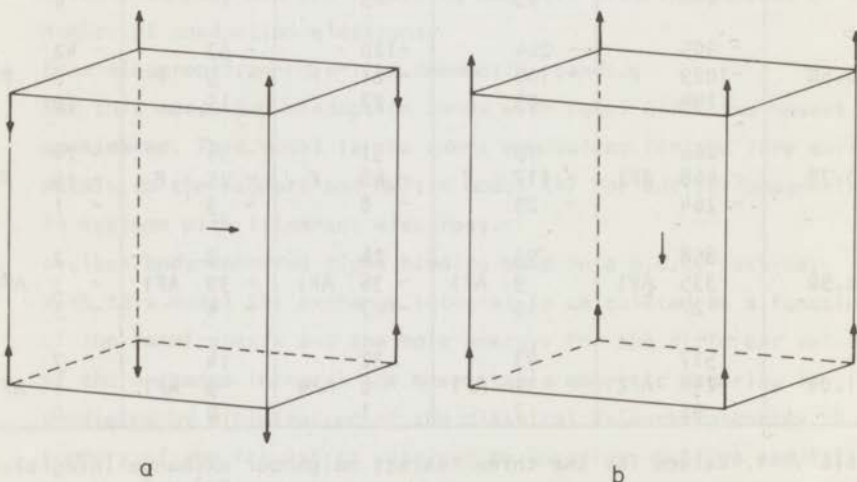
Fig. VI-2. *Expected types of antiferromagnetic ordering for $e_F = 1.00$ and $e_h = 0.10$ (a) and for $e_F = 0.80$ and $e_h = 0.30$ (b), according to the model of Gonçalves da Silva and Falicov.*

80

predicted. For larger values of e_h the influence of second nearest neighbour interactions is less, so the type of antiferromagnetic ordering of figure VI-2b is predicted. For an increasing number of conduction electrons here also the RKKY-type of interaction begins to dominate, finally resulting in a ferromagnetic ordering.

VI-3. Discussion.

As it is not possible to explain the magnetic behaviour of the rare earth chalcogenides having the thoriumphosphide structure in terms of the RKKY-theory, we will try to give an explanation for the different behaviour of the sulphides and selenides using the model of Gonçalves da Silva and Falicov. For instance, if we assume e_h to be approximately 0.30 - 0.50 for the sulphides, we expect a decreasing antiferromagnetic interaction with an increasing conduction electron concentration, that is with increasing e_F. When e_F equals approximately -0.70 we expect a ferromagnetic ordering to become stable. The expected value of e_h for the selenides will generally be smaller than that for the sulphides of the same composition due to the larger value of the band width (W) for the selenides. When we assume e_h for instance to be approximately 0.1 for the selenides we expect a strong antiferromagnetic interaction resulting in the antiferromagnetic ordering of figure VI-2a, due to the considerable contribution of next nearest neighbour interaction. For increasing values of e_F the contribution of next nearest neighbours relative to the nearest neighbours is reduced and the antiferromagnetic ordering of figure VI-2b is expected. When e_F equals approximately -0.50 a ferromagnetic ordering is expected. If these assumptions are correct, this behaviour will be reflected in the variations of the paramagnetic Curie-temperature with the composition. For the sulphides we expect a negative value for the paramagnetic Curie-temperature of L_2S_3 and ML_2S_4. With the number of conduction electrons increasing we expect the paramagnetic Curie-temperature to rise. In case of the selenides we also expect negative values for the paramagnetic Curie-temperatures of L_2Se_3 and ML_2Se_4. If our assumption of the value for e_h is correct the value of the paramagnetic Curie-temperature will become more negative with an increasing number of conduction electrons. When e_F reaches the value of -0.50 the RKKY-type interaction begins to

dominate and the paramagnetic Curie-temperature rises to positive
values.

With this model of Gonçalves da Silva and Falicov it will probably
be possible to explain the different magnetic behaviour of the rare
earth sulphides and selenides. To give a more quantitative discussion
of the magnetic behaviour of these compounds a more detailed knowledge
of the band-structures of these compounds is necessary. This informa-
tion is not available at present, but may probably be obtained by
measuring the electrical conductivity and optical properties of these
compounds.

References.

1. J.C. Eisenstein, R.P. Hudson, B.W. Mangum, Phys. Rev. (1965)
    137A, 1886.
2. C.E.T. Gonçalves da Silva, L.M. Falicov, J. Phys. (C) (1972)
    5, 63.
3. P.W. Anderson, Phys. Rev. (1950) 79, 350.
4. P.A. Fedders, P.C. Martin, Phys. Rev. (1966) 143, 245.

SAMENVATTING

Het doel van het in dit proefschrift beschreven onderzoek was een inzicht te verkrijgen in hoeverre de interactie tussen gelocaliseerde magnetische momenten via de electronen in de geleidingsband een rol kan spelen bij het magnetisch gedrag van de chalcogeniden van de zeldzame aardmetalen. In het bijzonder hebben wij hiervoor onderzoek verricht aan de zeldzame aardmetaalchalcogeniden met de thoriumfosfide structuur omdat het bij deze verbinding mogelijk is het aantal electronen in de geleidingsband onafhankelijk van de grootte van de kristallografische as te variëren.

In het eerste hoofdstuk wordt een overzicht gegeven van de diverse typen van magnetische interactie die bij metalen en metaalachtige verbindingen een rol kunnen spelen. Tevens wordt in dit hoofdstuk een aantal resultaten vermeld zoals die uit het werk van andere onderzoekers bekend zijn.

In het tweede hoofdstuk wordt de voor magnetische interactie in metalen belangrijke Ruderman en Kittel, Kasuya en Yosida-theorie bebesproken en wordt een relatie tussen de paramagnetische Curie-temperatuur en het aantal geleidingselectronen afgeleid. De in deze theorie voorkomende Ruderman en Kittel-som is voor het kationen rooster van de thoriumfosfide structuur berekend.

Het derde hoofdstuk geeft een overzicht van de in de zeldzame aardmetaalchalcogenide systemen voorkomende verbindingen en kristalstructuren. Van de in deze systemen veel voorkomende thoriumfosfide structuur wordt een beschrijving gegeven. Tevens is gezocht naar een mogelijke ordening van de kationen in de verbindingen $M(II)L(III)_2X_4$ en naar een ordening van vacatures in het kationen rooster van de metaal deficiente verbindingen met de thoriumfosfide structuur. Het voorkomen van dergelijke ordeningen was niet aantoonbaar. Wel kon worden aangetoond dat dergelijke ordeningen niet te verwachten zijn behalve voor de verbindingen $Eu(II)Eu(III)_2X_4$.

In het vierde hoofdstuk wordt een beschrijving gegeven van de voor dit onderzoek gebouwde, volledig geautomatiseerde apparatuur voor het meten van magnetische susceptibiliteiten.

Het vijfde hoofdstuk geeft de magnetische gegevens van de door
ons onderzochte verbindingen. Deze resultaten zijn niet geheel in over-
eenstemming met de RKKY-theorie.

In het zesde hoofdstuk wordt getracht aan de hand van de theorie
voor de magnetische interactie tussen zeldzame aardmetaalionen zoals
die is afgeleid door Gonçalves da Silva en Falicov de afwijkingen van
het volgens de RKKY-theorie verwachte magnetisch gedrag te verklaren.
Het blijkt mogelijk met bepaalde aannamen voor de breedte van de
geleidingsband, de Fermi-energie en de aanslagenergie van een 4f-electron
naar de geleidingsband een verklaring te geven voor het magnetisch gedrag
van deze verbindingen.

Op verzoek van de Faculteit der Wiskunde en Natuurwetenschappen volgt hier een kort overzicht van mijn academische studie.

Na het behalen, in 1959, van het einddiploma HBS-B aan het Rembrandtlyceum te Leiden begon ik in september van datzelfde jaar mijn studie in de scheikunde aan de Rijksuniversiteit te Leiden. Het candidaatsexamen, letter F, werd afgelegd in oktober 1963. De studie werd voortgezet onder leiding van de hoogleraren Dr. E.W. Gorter, Dr. E.C. Kooyman en Dr. W.M.H. Sachtler en de lector Dr. W.J.A. Maaskant.

Het doctoraalexamen met als hoofdvak anorganische chemie en als bijvakken organische chemie en heterogene katalyse werd afgelegd in oktober 1966.

Van april 1962 tot en met oktober 1966 vervulde ik een assistentschap bij de afdeling anorganische chemie. Van november 1966 tot en met december 1967 was ik als doctoraalassistent, vanaf januari 1968 als wetenschappelijk medewerker, en vanaf januari 1972 als wetenschappelijk medewerker I bij de afdeling anorganische chemie werkzaam, waar ik sinds augustus 1967 de taak van conservator vervul.

Na een onderzoek over de carbiden van de zeldzame-aardmetalen maakte ik in 1968 een begin met het in dit proefschrift beschreven onderzoek.

In 1973 legde ik met goed gevolg het examen voor octrooigemachtigde af.